REVISION 4

Degassing pathways of Cl-, F-, H-, and S-bearing magmas near the lunar surface: Implications for the composition and Cl isotopic values of lunar apatite

Gokce Ustunisik[1,*], Hanna Nekvasil[1], Donald H. Lindsley[1], and Francis M. McCubbin[2]

[1]Department of Geosciences, Stony Brook University, Stony Brook, New York 11794-2100, U.S.A.

[2]Institute of Meteoritics, Department of Earth and Planetary Sciences, University of New Mexico, Albuquerque, New Mexico 87131, U.S.A.

[*]**Present address:** Department of Earth and Planetary Sciences, American Museum of Natural History, New York, New York 10024-5192, U.S.A. E-mail: gustunisik@amnh.org

Abstract

Experimental degassing of H-, F-, Cl-, C- and S-bearing species from volatile-bearing magma of lunar composition at low pressure and f_{O2} close to the quartz-iron-fayalite buffer (QIF) indicates that the composition of the fluid/vapor phase that is lost changes over time. A highly H-rich vapor phase is exsolved within the first 10 minutes of degassing leaving behind a melt that is effectively dehydrated. Some Cl, F, and S is also lost during this time, presumably as HCl, HF, and H_2S gaseous species; however much of the original inventory of Cl, F, and S components are retained in the melt. After 10 minutes, the exsolved vapor is dry and dominated by S- and halogen-bearing phases, presumably consisting of metal halides and sulfides, which evolves over time towards F enrichment. This vapor evolution provides important constraints on the

geochemistry of volatile-bearing lunar phases that form subsequent to or during degassing. The rapidity of H loss suggests that little if any OH-bearing apatite will crystallize from surface or near surface (≈7m) melts and that degassing of lunar magmas will cause the compositions of apatites to evolve first towards the F-Cl apatite binary and eventually towards end member fluorapatite during crystallization. During the stage of loss of primarily H component from the melt, Cl would have been lost primarily as HCl, which is reported not to fractionate Cl isotopes at magmatic temperatures (Sharp et al. 2010). After the loss of H-bearing species, continued loss of Cl would result in the degassing of metal chlorides, which have been proposed as a mechanism to fractionate Cl isotopes (Sharp et al., 2010). After the onset of metal chloride degassing, the δ^{37}Cl of the melt would necessarily increase to +6 (82% Cl loss), +8 (85% Cl loss), and +20‰ (95% Cl loss) at 1, 4, and 6 hours, respectively, which was approximated using a computed trajectory of δ^{37}Cl values in basalt during degassing of $FeCl_2$. This strong enrichment of ^{37}Cl in the melt after metal chloride volatilization is fully consistent with values measured for the non-leachates of a variety of lunar samples and would be reflected in apatites crystallized from a degassing melt. Our results suggest that a range in δ^{37}Cl from 0 to > 20‰ is expected in lunar apatite, with heavy enrichment being the norm. While 95% loss in the initial Cl content of the melt (280 ppm Cl left in the melt) would cause an increase to +20‰ in δ^{37}Cl, the ability to measure this increase in a lunar sample is ultimately dependent upon the starting Cl abundances and whether or not a mechanism exists to concentrate the remaining Cl such that it can be subsequently analyzed with sufficient accuracy. Therefore, the higher the starting Cl abundances in the initial melts, the heavier δ^{37}Cl values that can be measurably preserved. Importantly, such enrichments can occur in spite of high initial hydrogen contents, and therefore, our experiments demonstrate that elevated values of δ^{37}Cl cannot be used as supporting evidence for an

anhydrous Moon. Furthermore, if the H-bearing vapor has a significant H_2 component, this process should also result in strong enrichment of δD in the residual magmas that reach the lunar surface or near-surface environment. Apatites within some mare basalts exhibit elevated δD of 1000 per mil depending on the initial value (Tartese and Anand 2013) in addition to the δ37Cl values, but elevated δ37Cl values are accompanied by only modest enrichments in δD in apatites from samples of the highlands crust (McCubbin et al. 2015a).

Keywords: Experimental degassing, Lunar magmas, Magmatic volatiles, Apatite, Chlorine isotopes, Hydrogen isotopes

Introduction

The recent success of detecting measurable amounts of hydroxyl in lunar apatite (Boyce et al. 2010; McCubbin et al. 2010a, 2010b; Greenwood et al. 2011; Barnes et al. 2013, 2014; Tartese et al. 2013, 2014), lunar volcanic glasses (Saal et al. 2008), including "melt" inclusions within olivine crystals of pyroclastic glass (Hauri et al. 2011), and in nominally anhydrous feldspar (Hui et al. 2013) has opened the door to a new paradigm of an H-bearing lunar interior. These observations also raise the obvious question, "How much H is in the lunar interior?" and, because of the importance of other volatiles such as F, Cl, and S, "What were the abundances of magmatic volatiles in lunar parental magmas?". The answers to these questions are not straightforward because degassing could have affected the initial magmatic volatile abundances during ascent. Furthermore, differential degassing of volatile species could have affected the relative abundances of volatiles in these melts (Ustunisik et al. 2011a). The potential for underestimating parental magma volatile contents is not restricted to glasses; apatites may also reflect volatile abundances of degassed melts, through either late-stage growth or modification of

pre-existing apatite. In fact, the mass balance calculations of Nekvasil et al. (2011) for the KREEP-bearing samples analyzed by McCubbin et al. (2010a) suggested that apatites record a degassing process that resulted in both loss of magmatic volatiles and significant changes in the relative volatile contents of the residual liquids, which may affect current interpretations of lunar apatite compositions (McCubbin et al. 2011). We conducted the first set of single-step degassing experiments (Ustunisik et al. 2011a) in order to determine the potential for differential degassing of volatiles of lunar magmas at shallow conditions. The single-step (6 hour) degassing experiments presented in Ustunisik et al. (2011a) determined the absolute and relative change in abundances of volatiles in the melt at shallow levels, simulating what might occur during rapid ascent of lunar magmas from depth without crystallization. Based on the initial and final abundances of the volatiles within the 6 hours of degassing, degassed samples with initially 2.2 and 2.5 wt% H_2Olost 99-100%H_2O, 89-84% Cl, 60-61% F, and 94-92% S respectively (Ustunisik et al. 2011a). These results showed that differential degassing resulted in changes in the relative abundances of volatiles (e.g., the F:Cl ratio) retained in the melt. In reflection of these changes in melt volatile contents, computed apatite composition changed from $Cl_{20}F_{48}OH_{32}$-apatite to $Cl_{10}F_{90}OH_0$-apatite ($D_F^{apat/basalt}$ =3.4, $D_{Cl}^{apat/basalt}$ = 0.8, Mathez and Webster 2005; $D_{H2O}^{apat/basalt}$ = 0.25, McCubbin et al. 2010a), that is, they reflected the dramatic decrease in magmatic water content as well as the decrease in Cl/F ratio. This result indicated that it is not only possible for lunar apatite from surface rocks to contain apatite that is grossly different from apatite in equilibrium with the magma prior to degassing, but use of such apatite compositions can lead to severely underestimated OH contents of the parental magma and underestimated magmatic Cl content. However, this investigation only looked at the final state of degassing; the path to that state remained unknown. Yet the path may indicate relative changes in

the degassing vapor along the route to that final state that could be expected if the process is arrested before completion (i.e., due to rapid cooling through the glass transition temperature), which could provide a guide for interpreting observations from lunar samples.

The degassing pathway may critically affect the compositional characteristics of apatite. It dictates the compositional evolution of apatite that crystallizes from a degassing magma. It also affects apatite compositional characteristics beyond the OH, F, and Cl contents, such as the Cl- and H-isotopic signatures. Sharp et al. (2010) noted a wide range of δ^{37}Cl values, from -1 to +24‰, in lunar materials that deviates substantially from the limited range of values exhibited by terrestrial samples, which are typically around 0‰ (Sharp et al. 2007, 2013b). They proposed that the enrichment of ^{37}Cl reflects kinetic loss of ^{35}Cl to the vapor phase in the form of metal chlorides such as NaCl, KCl, $MgCl_2$, and $FeCl_2$. Based on the strong enrichment of ^{37}Cl in the melt (and by extension, in the apatite crystallizing from such melt) they concluded that the parental magmas were anhydrous. Sharp et al. (2013a) later used the work of Ustunisik et al. (2011a, b) to hypothesize that high δ^{37}Cl values cannot rule out an earlier stage of preferential loss of H as H_2 before significant loss of Cl, although this idea has yet to be tested experimentally. Consequently, the primary objective of the present study is to experimentally determine whether or not degassing of H at low pressure can occur before substantial loss of Cl to reconcile the observations of elevated δ^{37}Cl values from rocks that also display evidence of elevated parental melt H_2O abundances.

Here a set of experiments were designed and implemented that focused on the degassing *pathway* of an OH-, F-, Cl-, and S-bearing lunar magma. In these experiments, changes in magmatic volatile-content were assessed from the initial state to the degassed state after specific degassing time intervals, and the vapor given off at each interval was computed based on mass

116 balance using the original volatile concentrations of the glass synthesized at high pressure and
117 the residual glass that was analyzed at the end of each degassing time step. The change in vapor
118 composition during degassing was then used to compute the effect of degassing on the Cl
119 isotopic values.
120
121 ## Experimental procedures
122 ### Experimental design
123 The experiments simulated the scenario of volatile-bearing melt formation at depth (100
124 km) followed by rapid ascent to the lunar surface (≈7m) where devolatilization did not occur
125 until low pressure (<1 bar). The experiments were also conducted at low oxygen fugacity, close
126 to the QIF buffer, to match the approximate oxygen fugacity of lunar magmas (Taylor et al.
127 2004). The synthetic composition used in Ustunisik et al. (2011a) (high-Al basalt 14053 Willis et
128 al. 1972) was also used in the present study to facilitate direct comparison between both studies.
129 High-Al basalt 14053 was selected for a number of reasons. Its bulk composition is likely
130 reflective of a liquid composition (Neal and Kramer 2006). Additionally, it is close in
131 composition to terrestrial tholeiites, so its degassing behavior can also be compared to terrestrial
132 basalts. Furthermore, 14053 is among the most well-studied samples in the lunar collection (Neal
133 et al. 1989; Taylor et al. 2004). The volatile contents of the synthetic 14053 (0.5 wt% Cl, 0.5
134 wt% F, 0.3 wt% S and 2.3 wt% water) were selected to ensure that analytical uncertainty does
135 not inhibit detection of changes in volatile concentration.
136 Volatile-bearing glass was synthesized at 0.5 GPa and 1400 ^{0}C in graphite capsules.
137 Quenched glass from the high pressure synthesis experiments was analyzed for volatile content
138 by micro-FTIR (for H_2O) and electron probe micro analysis (major elements and F, Cl, and S) to

ensure that the volatile content obtained was that intended in the synthesis. These analyses provided confirmation that loss of volatiles during the quench from the high pressure synthesis conditions did not occur. For the low pressure degassing, care was taken to select synthesized glass pieces that were free of visible graphite (as determined by binocular inspection). However, in view of the likelihood that C-O-H species were present in lunar magmas (e.g., Sato 1979; McKay and Wentworth 1992; Fogel and Rutherford 1995; Rutherford and Papale 2009; Wetzel et al. 2013), small amounts of graphite and any dissolved C-O-H species retained after quench of the original glass were deemed acceptable in the starting material for the degassing experiments. The experimental conditions for degassing included a maximum pressure of approximately one third of a bar, superliquidus temperatures, and selected specific time intervals of 10 minutes, 1 hour, 4 hours, and 6 hours. The degassing experiments were specifically conducted in long evacuated silica glass tubes in order to build up a small partial pressure of exsolved gases locally and to slow the effects of Rayleigh distillation that would come from boiling in an unconfined system. The length of the vacuum-evacuated silica glass tube was computed to provide up to 1/3 of a bar pressure during the experiment, based on the amount of glass loaded, the volatile content of that glass, the assumption of complete loss of all volatiles from the glass, the average temperature in the tube, and the assumption of ideal mixing of *components* in the vapor phase at high temperature. Since temperature varied along the length of the silica glass tube, the pressure was approximated using the average temperature (725 ^{0}C). The actual pressure within the experimental charge likely varied along with the thermal gradient such that the cooler regions of the charge likely had lower pressure, resulting in the deposition of the volatile components on the walls of the sealed silica glass tube.

This experimental setup was designed to simulate degassing under lunar conditions where a degassed vapor cloud expands, cools, and deposits vapor components in the cooler regions, which drives further devolitilization from the magma in contact with the vapor (Saal et al., 2008, Elkins-Tanton et al., 2003; Colson, 1992). Consequently, the degassing is occurring in an analogous manner to what would be expected during Rayleigh fractionation, but the fractionation is much slower than it would be in an unconfined open system like that provided by a gas-mixing furnace with a continuous gas flow. Additionally, this experimental design allows for the degassing path to be observed at longer time scales than would be provided by unconfined open-system degassing.

In previous experiments (Ustunisik et al. 2011a), the final degassed state was reached by 6 hours of degassing at low pressure, that is, no further changes were detected for longer degassing duration. For this reason, degassing periods were less than or equal to 6 hours in the present study. However, in order to ensure that 6 hours of degassing was sufficient to achieve a final state and not a path-dependent intermediate step, an additional experiment was conducted in which the partially degassed glass was quenched after 4 hours and then used for an additional 2-hour degassing experiment. Also, partially degassed glass that was quenched after 1 hour of degassing was used for an additional 3-hour degassing experiment to reach a total of 4-hours of degassing. Since 4-hours is not the final state in degassing, we expect to see slight differences between two-step 1+3h and one-step bulk 4h experiments.

Experimental details

High-pressure hydrous glass synthesis. The volatile bearing glass that was used as starting material for the degassing experiments was synthesized at 0.5 GPa in order to ensure significant

184 volatile solubility to mimic the state of a lunar magma that would be coming from depth. This
185 target composition is presented in Table 1. The starting material was produced from a mixture of
186 oxides and silicates by homogenizing the mixture in ethanol in an automatic mortar for 2 hours.
187 Brucite was added such that the mix would have ~2.3 wt% water; $MgCl_2$, MgF_2, and $CaSO_4$ were
188 added in the last stage and the mixture ground by hand (using minimal amounts of ethanol)
189 before drying at 175 ^{0}C under vacuum to remove adsorbed water. Hydrous glass was synthesized
190 by melting this powder in a graphite capsule, which was inserted, with dried pyrophyllite
191 spacers, into a graphite furnace that was inside of a talc sleeve. The sample was pressurized in a
192 piston-cylinder apparatus at 0.5 GPa and heated to 1400 ^{0}C for ~2 hours to ensure complete
193 melting before quenching and analysis.
194 **Low-pressure evacuated silica glass tube experiments.** Irregular glass fragments were
195 obtained at the end of synthesis experiments and ranged in size from 5 to 450 μm. From these
196 sizes, glass fragments in the range of 300 to 450 μm were selected for 10 min, 1 hour, 4 hour, 6
197 hour, 1+3 hour, and 4+2 hour degassing experiments. Similar sizes of glass fragments were
198 chosen in order to normalize any effects of sample size and/or surface area on the degassing rate.
199 Selected pieces of the volatile-bearing glasses were placed in Fe^0 capsules with slotted lids and
200 inserted into long silica glass tubes, sealed at one end. Each tube was evacuated for 20 minutes
201 before completely sealing it. Subsequently, the sealed tube was inserted rapidly into a preheated
202 vertical Pt-wound furnace such that the sample was in the hotspot. The sample was kept entirely
203 in the "isothermal" zone throughout the duration of each experiment. This isothermal zone was
204 determined for the furnace prior to our experimental work. Maintaining a low pressure in spite of
205 devolatilization was facilitated by use of a long silica glass tube; however, this resulted in the
206 tube not being fully contained in the isothermal zone. This thermal gradient in the overlying

207 silica glass tube (1250 ^{0}C at the hot spot and 200 ^{0}C at the uppermost end) made it impossible to
208 collect, analyze or computationally predict the composition of the vapor phase directly. But the
209 isothermal condition of the melt allowed for careful evaluation of the loss of volatiles from the
210 melt. The sample was held at 1250 ^{0}C (that is, above the low pressure liquidus temperature in
211 order to avoid crystallization) for selected time intervals. Time was measured after the furnace
212 regained the set temperature which typically took 10 minutes. Consequently, the shortest
213 experiment duration that we could run was 10 minutes, using our experimental setup. Sublimates
214 were formed on the interior walls of the silica glass tube well above the sample. We did not
215 make predictions regarding the identity of the phases that precipitated from the vapor due to the
216 variable temperature, pressure, and oxygen fugacity within the region that those phases
217 precipitated, although we note that their identity is not a requirement for determining the volatile
218 evolution of the degassing vapor and silicate melt. The presence of a lid on the capsule protected
219 the melt to a great extent from mechanical mixing with any sublimates that were released from
220 the walls and settled downward gravitationally. Each experiment was quenched by dropping the
221 capsule-bearing end of the silica glass tube into cold water.

222 For the single-step degassing experiments (i.e., degassing of the initial bulk composition)
223 the initial glasses were heated above the liquidus temperature for 10 minutes, 1 hour, 4 hours,
224 and 6 hours before quenching. For the sequential two-step degassing experiment, partly degassed
225 glass at the end of 1 hour was used for degassing an additional 3 hours to reach a nominal total of
226 4 hours of degassing. Similarly, partly degassed glass at the end of 4 hours was used for
227 degassing an additional 2 hours to reach a final state of 6 hours of degassing. These experiments
228 were used to verify the "final state" of degassing, determined previously by Ustunisik et al.,
229 (2011a) to be 6 hours.

Analytical techniques

Pieces of both the crystal-free glass at the end of synthesis and the degassed glasses after the degassing experiments were sliced and prepared as polished mounts for electron probe micro analysis and as free hanging doubly polished wafers for micro-Fourier transform infrared spectroscopy (micro-FTIR) analysis. Polished probe mounts were characterized using a petrographic reflected light microscope at Stony Brook University and JEOL 8200 electron microprobe at the Institute of Meteoritics at the University of New Mexico. Qualitative analysis was performed using both backscattered electron imaging and energy dispersive spectroscopy. Quantitative analyses were performed using wavelength dispersive spectrometers. An accelerating voltage of 15 kV and a nominal probe current of 20 nA was used during each analysis. We analyzed for the elements Si, Ti, Al, Fe, Mn, Mg, Ca, Na, K, P, S, F, and Cl. F was analyzed using a synthetic light-element LDE1 detector crystal, and the peak was measured in differential mode to avoid the F*K*α peak overlap with the shoulder of the Fe*L*α peak (i.e., Witter and Kuehner 2004). SrF_2 was used as a fluorine standard, and the standardization was checked against a terrestrial kaersutite from Spitsbergen with 1300 ppm F (McCubbin et al. 2015b), measured previously by secondary ion mass spectrometry. Si and Mg were standardized using a synthetic diopside crystal. Ti, Fe, and Mn were standardized using ilmenite. Al and Ca were standardized on anorthite; Na and K were standardized on albite and orthoclase, respectively. A natural fluorapatite from India (Ap020 from McCubbin et al. 2012) was used to standardize P; and Cl was standardized using sodalite. S and Ba were standardized using Taylor barite. In order to reduce or eliminate electron beam damage, a 10 μm spot was used for both standardization and analysis of glass in all the experimental samples. Tests on several secondary standards were

253 performed throughout the analytical session to verify that standardizations did not drift. The
254 average glass composition for the starting composition is shown by the composition labeled
255 initial (t0) in Table 1.

256 Water analysis of the starting glass as well as of the degassed glasses was conducted by
257 micro-FTIR on doubly polished free-hanging glass wafers using a Nicolet iN10MX FTIR
258 microscope equipped with a liquid nitrogen-cooled MCT array detector in the Department of
259 Geosciences, Stony Brook University. Total water concentrations were based on the intensity of
260 the broad band at 3570 cm^{-1} and a molar absorptivity of 62 L/mol*cm via the method of Dixon et
261 al. (1995) and Mandeville et al. (2002). Both the spectrometer and the IR objective were purged
262 with dry nitrogen gas at a rate of 15 L/min. Transmittance IR spectra were collected using a KBr
263 beam splitter, MCT/A detector, and a globar source. Approximately 400 scans were performed
264 for each IR spectrum acquired at a spectral resolution of 8 cm^{-1} over a spectral range of 4000-
265 715 cm^{-1}. Peak heights were determined using the Omnic Picta software. Backgrounds were
266 collected before each analysis and under the same conditions of air and ambient temperature as
267 the analyses. The stated uncertainty (Table 1) arose primarily from thickness variations within
268 the individual wafers.

269 **Experimental results**

270 **Geochemical observations**

271 After degassing and quench, the silica glass tube showed some devitrification and
272 precipitate formation around the Fe^0 capsule at one end, and rings of reaction precipitate some
273 distance from the capsule. The capsule remained shiny in each experiment, suggesting that the
274 silica glass tube retained its integrity for the duration of the experiment. The degassed samples
275 consisted of glass, irregular blobs of metallic iron, and large vesicles (rare). Figure 1 shows the

back-scattered electron (BSE) images of initial and final glasses after 10 minutes, 1 hour, 4 hours, and 6 hours of bulk and 1+3 hour and 4+2 hour two-step (sequential) degassing. Irregular metallic iron blobs were only found in 1, 4, 6, 1+3, and 4+2 hour degassing experiments (Fig.1).The compositions of the initial and final degassed glasses are given in Table 1. Each run product analysis shown is the average of 9 electron microprobe analyses. The 1σ value presented parenthetically represents the standard deviation of the mean for each oxide value, which was larger than the analytical uncertainty determined by counting statistics.

The glass produced at 10 minutes of degassing showed complete loss of all H_2O and did not show evidence of either loss or gain of FeO. This latter observation may seem counterintuitive, since the sample synthesis took place at higher fO_2 than the degassing experiments. The establishment of a lower ferric:ferrous Fe ratio in the melt would be expected to release oxygen, which would react with the Fe^0 capsule to produce FeO. This FeO would dissolve in the silicate melt and reasonably cause a net increase in the FeO_T in the melt. However, the residual graphite in the glass (from the high pressure synthesis in graphite) may have reacted with the oxygen released during this reduction to produce CO. Similarly, graphite could also have become oxidized from the oxygen residual to hydrogen loss during degassing (loss of water component). Some amount of C could have been lost to methane production. Taken together, these reactions could impede the oxidation of the Fe^0 capsule and the addition of Fe to the melt.

In contrast, for each of the longer duration degassing experiments there was a significant loss of FeO component from the melt (cf. initial and final compositions of Table 1) that was correlated with the development of metallic Fe droplets along the interior walls of the capsule. This was presumably due to continued oxidation of graphite through the reaction

299 $FeO(m) + C \rightarrow Fe^0 + CO(g)$

300 In the absence of water that provided oxygen for the oxidation of C, this resulted in considerable
301 reduction of FeO in the melt.

302

303 **Mass balance calculations**

304 Determining the amount of volatiles lost from the melt is complicated by the change in
305 silicate melt composition resulting from the formation of metallic iron by FeO reduction. The
306 decrease in amount of silicate melt would lead to an apparent lower computed amount of volatile
307 loss. For this reason, mass balance calculations were conducted in order to convert the system
308 back onto a metallic Fe-free basis.

309 The proportion of phases (melt, vapor, and metallic Fe) was determined by mass balance
310 through correction of the major oxide constituents of the final degassed melt for FeO_T loss due to
311 iron reduction as discussed previously (Ustunisik et al. 2011a). The weight fraction of silicate
312 melt after degassing (WFm) was computed for each likely refractory oxide (CaO and MgO) as
313 the weight ratio in the initial and final (degassed) silicate glasses. The actual WFm used (and
314 listed in Table 2) lies between the values obtained from CaO and MgO and was chosen because
315 it yielded the best overall mass balance for each experiment. The weight fraction of FeO lost as
316 Fe^0 and oxygen ($WFFeO^r$) was computed as

317 $$WFFeO^r = (FeO^{\text{initial melt}} - WFm*FeO^{\text{final melt}})/100,$$

318 and the degassed glass composition was corrected for this.

319 The WFm and $WFFeO^r$ can be used to obtain the weight fraction of vapor (WFv) through
320 the relation

321 $$WFv = 1 - (WFm + WFFeO^r).$$

With the consideration of only the chemical components water, Cl, F, and S , the composition of the vapor phase and the percentage volatile loss are

$$i^{v} = (i^{\text{initial melt}} - WFm * i^{\text{final melt}})/WFv$$

$$\%\ i\ \text{lost} = 100*(i^{\text{initial melt}} - WFm * i^{\text{final melt}})/i^{\text{initial melt}}$$

respectively, where i^{v} is the wt% of component i in the vapor, and $i^{\text{initial melt}}$ and $i^{\text{final melt}}$ are in wt%. The percentage volatile loss for 1+3 h and 4+2h segment of sequential degassing was calculated with the formula above used for bulk degassing, where the initial melt is the melt at the end of1 h and 4h bulk degassing and the final melt is the melt at the end of1+3h and 4+2h sequential degassing respectively. The extent of overall degassing for the time segment 1+3h and 4+2h (for comparison with the bulk degassing) is % i lost = % i lost at the end of 1h or 4h + (% i left at the end of 1h or 4h * % i lost between 1+3h and 4+2h respectively). The results of mass balance calculations for each time interval during bulk and sequential degassing are given in Table 2.

The loss of FeO from the melt has been computationally attributed here to Fe^{0} production and calculated through $WFFeO^{r}$. This computation ignores the loss of Fe through the formation of iron halide vapor species such as $FeCl_2$, which would contribute to the mole fraction of vapor phase (Xv). This exclusion of iron halide vapor would only cause a potential problem after degassing for 10 minutes, since before this there was no detectable Fe loss. In the later stages of degassing after all H_2O component is lost, from 10 minutes to 1h , 1h to 4h, and 4+2h significant changes in total FeO content occurred by reduction. In the absence of H remaining in the melt, the loss of Cl was likely in the form of metal chloride vapor complexes, and most likely Fe chloride complexes. Thus, some of the observed FeO loss should be attributed to vapor phase production. However, the Wfv is only 0.004, 0.001, 0.003 of the total system during 10min to

345 1h, 1+3h, and 4+2h portions of degassing, respectively; therefore, the neglected Fe loss to the
346 vapor as $FeCl_2$ has a negligible effect on the computed vapor abundance.
347
348 **Degassing of volatile components**
349 As shown in Figure 2, after 10 minutes degassing, there was complete loss of water
350 component and loss of about 66% Cl, 38% F, and 70% S to the vapor phase. Between 10
351 minutes and 6 hours there was a nearly linear loss of volatiles at the rate of approximately 4%
352 per hour for each of the remaining volatile components. For the longest degassing period (6
353 hours), the percentage loss was 100% water, 95% Cl, 71% F, and 96% S component from the
354 initial melt to the vapor phase. The extent of overall loss in the two-step degassing, 4 hours then
355 2 additional hours (t4+2h), was computed to be 95% Cl, 64% F, and 95% S respectively
356 (Fig.2). The smaller extent of loss of F in this two-step process in 4+2h (symbols with gray
357 outlines in Fig. 2) suggests that the quenching and re-heating process required additional time to
358 attain the same extent of degassing. The intermediate nature of the extent of degassing in the
359 two step process between 4 and 6 hours can also be seen in the melt volatile contents in Table 2.
360 By examination of the volatile loss curves of Cl and S (Fig. 2), it is approximated that the
361 sequential degassing of 4+2h was the equivalent of approximately 5.4 h bulk (single-step)
362 degassing.
363 The extent of overall loss in the earlier portion of two-step degassing, 1 hours then 3
364 additional hours (t1+3h) was computed to be 94% Cl and 66% F (Fig.2). The higher extend of
365 loss of Cl, F, and S for 1+3h two-step process compared to 4h bulk degassing indicates the
366 kinetics of degassing being highly path dependent between 1+3h degassing since 4h is still not
367 the final state of degassing.

368 The change in volatile phase over each time increment of degassing was computed and is
369 shown schematically in Figure 3 and in detail in Figure 4. As discussed in Ustunisik et al.
370 (2011a), the volatile phase compositions calculated here through mass balance indicate the
371 component abundances only; the gas species likely consisted of HCl, HF, H_2S, CO (from
372 graphite), NH_3 (from residual trapped air), H_2, and some H_2O. At fO_2's relevant to lunar
373 volcanism (i.e., IW-1; Herd et al. 2008), H_2O would make up a minor component of the
374 degassed vapor in the O-H system, with the dominant vapor species being H_2 (Elkins-Tanton
375 and Grove 2011); however, it has been shown experimentally at elevated pressure and at low H
376 concentrations that the silicate melt would have had mostly OH- species (Hirschmann et al.
377 2012). Consequently, the conversion of water (OH-) to H_2 may have facilitated the thorough
378 loss of the water component from the melt during degassing (Zhang and Ni 2010).
379 The vapor given off at 10 minutes also contains Cl, F, and S. The higher Cl:F ratio in this
380 first vapor phase compared to the initial melt is indicated by the greater drop in melt Cl content
381 than F content in the degassed melt. Higher Cl/F ratio in the initial vapor phase is also consistent
382 with the different roles that F and Cl play in the melt structure (Baker and Balcone-Boissard
383 2009) as F replaces coordinating oxygen while Cl associates with water and alkali cations and
384 possibly forming a Cl-alkali-H_2O outside of a melt structure (Schaller et al. 1992; Zeng and
385 Stebbins 2000; Liu and Nekvasil 2002; Mysen et al. 2004; Sandland et al. 2004; Kiczenski and
386 Stebbins 2006). If the halogen-bearing vapor species formed are HF and HCl, then this indicates
387 a higher volatility of the HCl species under water-rich conditions, as is reflected in its lower melt
388 solubility (e.g., Carroll and Webster 1994; Webster et al. 1999; Signorelli and Carroll 2000,
389 2002; Webster and De Vivo 2002). If S is given off as H_2S, the H_2S has about the same volatility
390 as HCl under H-rich conditions. After 10 minutes of degassing, the water content is less than

391 0.01 wt%, and the volatile phase given off is very different from the initial H-rich composition.
392 The dry volatile phase has a Cl:F:S ratio of approximately 8:7:6, although when these values are
393 normalized to the respective Cl, F, and S concentration in the melt, the Cl:F:S ratio is
394 approximately 18:5:33. This result indicates that S is more volatile than Cl, and Cl is more
395 volatile than F during degassing under lunar conditions. Eventually, as the abundance of Cl and
396 S decrease in the melt, the volatile phase given off at the last stages is dominated by F (Fig. 4).
397 Figure 5a shows the relative changes in OH, F, and Cl in the melt and Figure 5b shows in
398 the computed volatile phases. This emphasizes that the low pressure degassing path is one of
399 early extensive loss of H-species with some halogen loss, followed by likely metal halide loss
400 with a greater loss of Cl than F from the melt.
401
402 **Comparison between experimental observations and known diffusivities for F, Cl, S, and**
403 **H_2O**
404 Although little is known regarding the diffusivities of H_2O, H_2, F, Cl, and S (sulfide)
405 components in silicate liquids, there are some estimates available (e.g., Watson, 1994; Alletti et
406 al., 2007; Baker and Balcone-Boissard, 2009; Dingwell and Scarfe, 1985; Zhang et al., 2010;
407 Zhang and Ni, 2010). Under the conditions of our experiments (basaltic liquids at <1bar and
408 1250 ^{o}C), diffusion coefficients (D) for H_2O, Cl, F, and S^{2-} components were calculated and
409 summarized in Table 3. Several of the diffusion coefficients were dependent upon the H_2O
410 content of the melt, and so D was calculated for the initial 10 minutes (assuming the starting
411 H_2O content of 2.3 wt.% H_2O) as well as post 10 minutes (where H_2O abundances were
412 approximately 0.01 wt.% H_2O). Based on the reported diffusivities for the initial 10 minutes,
413 H_2O diffuses faster than F, which is faster than Cl, which is faster than S with an H:F:Cl:S D

ratio of 850:20:16:5. After initial loss of most H (after 10 minutes), F diffuses faster than Cl, which diffuses faster than H, which diffuses faster than S with an H:F:Cl:S D ratio of 6:17:9:3. Based on these results, we conclude that we cannot explain the experimentally observed degassing path strictly by end member diffusion. In a system controlled by diffusive loss, the vapor would have evolved to Cl and S rich compositions rather than F-rich compositions as observed.

Discussion

Evolution of apatite compositions during degassing

Apatite volatile contents reflect those of the magmas from which they crystallize. The changes in relative volatile content during shallow magmatic degassing will strongly affect the composition of apatite crystallizing before or after degassing. Figure 5c shows hypothetical apatite compositions calculated for the initial melts and progressively degassed melts using exchange K_D values for the volatiles between apatite and basaltic liquid ($K_D^{F\text{-}Cl}{}_{Ap/Liq}$=0.20, $K_D^{F\text{-}H2O}{}_{Ap/Liq}$=0.01, $K_D^{Cl\text{-}H2O}{}_{Ap/Liq}$=0.04, McCubbin et al. 2013; 2015b; Boyce et al. 2014) during various intervals of bulk degassing. The apatites from the degassed magmas would not only be very low in OH but also have a higher F:Cl ratio than apatites crystallized prior to degassing, as suggested by McCubbin et al. (2011). The ease with which the water component is lost from the melt suggests that apatite formed during degassing would mainly show variable F:Cl ratios but low OH contents. Although rapid ascent has been called upon for some lunar lithologies (i.e, melts that produced the pyroclastic glasses), for a given ascent rate, lunar magmas experience a smaller change in pressure with time relative to terrestrial magmas, making it more likely that extensive degassing will occur before the surface is reached and late-stage apatite crystallizes.

437 The late-stage of apatite crystallization in most magmas suggests that few hypabyssal or
438 extrusive rocks should contain apatite that has preserved the initial volatile composition of the
439 parental magma. Instead, these apatites should primarily preserve evidence of the residual post-
440 degassing volatile composition. This process would be exascerbated by secondary processes like
441 impact melting, which could cause melting and recrystallization of apatite that would
442 subsequently reflect the volatile composition of the impact melts (e.g., Treiman et al., 2014).
443 This assertion is supported by electron probe micro analysis of apatite from impact melts that
444 show monovalent anion sites with their stoichiometric fill by F + Cl and hence no evidence for a
445 missing structural component that could be attributed to OH^- (i.e., McCubbin et al. 2011, Barnes
446 et al., 2014; Robinson and Taylor, 2014).

447 Apatites zoned in volatile contents such as described for 15404 and 14053 by Nekvasil et
448 al. (2011) suggest the possibility of crystallization of apatite from volatile-bearing magmas at
449 depth, followed by eruption, followed by impact gardening, and finally impact heating that
450 results in exchange of volatiles from the exterior of the apatite grains.This same variable
451 distribution in apatite chemistry has also been predicted to occur in apatites that crystallize
452 fractionally where apatite is part of the fractionating assemblage (Boyce et al. 2014); however, in
453 the fractional crystallization scenario apatite evolves towards OH-rich compositions as opposed
454 to the F-rich compositions predicted from degassing. Consequently, so careful detail to textural
455 associations of apatite as well as timing of crystallization is required to accurately interpret
456 apatite volatile abundances and their relation to the volatile abundances of the parent liquids.

457

458 **Implications for Cl isotopes**

Sublimates have been found in lunar pyroclastic deposits as coatings on soils and individual glass beads (e.g., Meyer et al. 1975; Colson, 1992; Elkins-Tanton et al., 2003). These sublimates contain both sulfides and chlorides, including NaCl, $ZnCl_2$, $FeCl_2$ (e.g., Bell 1974). The potential Cl isotopic effect of the degassing process that produced these metal chlorides was investigated by Sharp et al. (2010) by measuring the Cl isotope abundances in several lunar basalts, volcanic glasses, and apatite grains and looking at the differences in $\delta^{37}Cl$ in leachates vs. residual rock. They found a large difference between the water soluble Cl (with lower $\delta^{37}Cl$) and the structurally bound Cl (relatively higher $\delta^{37}Cl$) in several samples, and they attributed this difference to degassing rather than surface processing. They linked the loss of ^{35}Cl to the loss of metal chloride vapor species rather than HCl, the latter of which, using terrestrial analogs, they note results in only minor isotopic fractionation between melt and vapor at magmatic temperatures. Sharp et al. (2010) point out that the formation of metal halide vapor species is predicted from thermodynamic calculations for conditions under which the Cl/H ratio is substantially greater than 1 (Fegley and Swindle 1993).

The nearly bimodal volatile phase compositions computed from these degassing experiments has major implications for lunar Cl isotopic compositions. The early loss of essentially all water and some Cl and F from the melt suggests the likely formation of HCl and HF vapor species early and therefore, no isotopic effect during this initial degassing stage. However, subsequent to rapid H loss, a halide phase with essentially no H-bearing species would result in very strong isotopic fractionation, with strong enrichment in ^{37}Cl in the melt and therefore, in the apatite that formed from it. If loss of the H-rich vapor is much faster than the loss of the halogen-rich phase, as suggested by these experiments, then low-pressure late-stage

apatite would form primarily after water degassing and show therefore, mainly OH-free compositions, regardless of the initial water content.

The change in Cl isotopic composition of the melt after the loss of water and during the degassing of metal chlorides can be approximated using the computed trajectory of $\delta^{37}Cl$ values in basalt during degassing of $FeCl_2$ (likely to be a major volatile constituent) from Sharp et al. (2010). Figure 6 shows the fraction of Cl remaining in the melt after each degassing experiment relative to the melt Cl content after 10 minutes degassing. It is anticipated that metal chlorides will not have vaporized to any significant extent before 10 minutes of degassing as that is the period of water loss and the likely formation of HCl species. Therefore, the Cl isotopic signature will have stayed at its initial value of approximately zero per mil (Sharp et al. 2010) during the first 10 minutes. As shown in Figure 6, the loss of the volatile chlorides at 1, 4, and 6 hours, however, would yield a $\delta^{37}Cl$ of +6, +8, and +20‰, respectively, in the residual melt. This strong enrichment of ^{37}Cl in the melt after metal chloride volatilization is fully consistent with values measured by Sharp et al (2010) for the non-leachates of a variety of lunar samples. Unless there is some unexplained isotopic effect between melt and apatite, it is anticipated that the computed ^{37}Cl enrichment of the residual melt, based on these experiments (Fig. 6), would lead to the degree of enrichment of ^{37}Cl in apatite compositions observed by Sharp et al. (2010) for the mare basalts and mare basalt apatites. $\delta^{37}Cl$ values for the lunar highlands apatites and apatites in some impact melts are considerably higher (+25 to +80‰; Sharp et al. 2010; Wang et al. 2012) and may require secondary processing and melting to reach the observed $\delta^{37}Cl$ values through degassing of metal chlorides.

The experiments indicate that strong enrichment of $\delta^{37}Cl$ can occur in magmas that were initially quite hydrous, therefore positive $\delta^{37}Cl$ values relative to SMOC cannot be used to

support the concept of an anhydrous Moon. These findings are in agreement with the hypothesis of Sharp et al. (2013a). The presence of such Cl isotopic signatures however, may be restricted to the surface and shallow subsurface because low pressures (<1 bar) are required for the extreme disparity between the compositions of initial and later-formed (≥10 minutes of degassing) volatile phases. Furthermore, loss of the H component from the melt primarily as H_2 would result in high δD values (as noted by Saal et al. 2013, Sharp et al. 2013a, and Tartese and Anand 2013), and may explain in part some of the marked heavy isotopic enrichments described for lunar apatite by Greenwood et al. (2011), Barnes et al. (2013, 2014), and Tartese et al. (2013, 2014), although it is not clear that degassing is the sole factor controlling H isotopes (Greenwood et al., 2011, McCubbin et al. 2015a).

Controls on degassing pathway

Several factors can control the evolution of the vapor species and residual melt during degassing including diffusion within the silicate melt, direct exsolution of volatile components into the vapor phase, or nucleation of bubbles within the melt, all of which likely played some role in our experiments. Importantly, our experimental results could not be predicted by published diffusion coefficients for each of the volatile components. In fact, based on the available diffusion coefficients, apatite compositions during degassing would have evolved towards the chlorapatite apex after hitting the F-Cl join instead of towards the fluorapatite apex like was observed in our experiments and in natural lunar apatites (McCubbin et al., 2011; Tartese et al., 2014). Consequently, we conclude that the published diffusivities for F, Cl, and S may not be appropriate for the conditions of our experiments, which are at lower pressures and oxygen fugacities than much of the previous experimental work. Furthermore, our experiments

were conducted using a high-Al lunar basalt, whereas the diffusion coefficients were derived from terrestrial basalt compositions. Alternatively, the degassing of our experiments was predominately controlled by other factors such as solubilities of the individual melt components where super-saturation resulted in rapid loss due to bubble nucleation or direct exsolution from the melt into the vapor phase. Regardless of which is the case, this comparison illustrates the importance of conducting experiments over using solely a modeling approach.

Implications

Recent determinations of OH in lunar apatite have spurred the desire to use apatite to infer volatile contents of lunar magmas and magmatic source regions. The isotopic composition of volatiles ($\delta\ ^{37}Cl$ and δ D values) within these apatites have been used to evaluate the implications and processes involved in reshaping a new lunar paradigm of lunar volatiles. This work successfully addresses three key issues within this context. The first is the extent of degassing and how it may influence apatite growing before or after degassing; the second reconciles observed enrichments of ^{37}Cl and D with a "hydrous" lunar mantle. Lastly, the presence of Cl- and S-rich reduced fluids in the lunar crust have been recently implicated for causing alteration and sulfide replacement textures in several lunar crustal samples (Shearer et al., 2012, 2014, 2015; McCubbin et al., 2015a; Elardo et al., 2012), consistent with the similar volatilities of both elements as observed in this study.

Acknowledgments

Support for this work was provided by the NASA Lunar Advanced Science and Exploration Research (LASER) grant NNX08AZ04G to HN. FMM acknowledges support from the NASA

549 Lunar Advanced Science and Exploration Research (LASER) grant NNX13AK32G to FMM and
550 NNX11AB30G to Carl Agee during this study Authors benefitted greatly from the detailed and
551 constructive comments by Zachary Sharp, and three anonymous reviewers. We are also grateful
552 for time and effort put forth by the AE Peter Isaacson.

553

554

555 **References cited**

556 Alletti, M., Baker, D.R., and Freda, C. (2007) Halogen diffusion in basaltic melt. Geochimica et
557 Cosmochimica Acta, 71, 3570-3580.

558 Baker, D.R., and Balcone-Boissard, H.B. (2009) Halogen diffusion in magmatic systems: Our
559 current state of knowledge. Chemical Geology, 263, 82-88.

560 Barnes, J.J., Franchi, I.A., Anand, M., Tartèse, R., Starkey, N.A., Koike, M., Sano, Y., and
561 Russell, S.S. (2013) Accurate and precise measurements of the D/H ratio and hydroxyl
562 content in lunar apatites using NanoSIMS. Chemical Geology, 337, 48-55.

563 Barnes, J.J., Tartèse, R., Anand, M., McCubbin, F.M., Franchi, I.A., Starkey, N.A., and Russell,
564 S.S. (2014) The origin of water in the primitive Moon as revealed by the lunar highlands
565 samples. Earth and Planetary Science Letters, 390, 244-252

566 Bell, P.M., El Goresy, A., and Mao, H.K. (1974) A study of iron-rich particles on the surfaces of
567 orange glass spheres from 74220. Proceedings of 5th Lunar and Planetary Science
568 Conference, p. 187-191.

569 Boyce, J.W., Liu, Y., Rossman, G.R., Guan, Y., Eiler, M.J., Stolper, E.M., and Taylor L.A.
570 (2010) Lunar apatite with terrestrial volatile abundances. Nature, 466, 466-469.

571 Boyce, J.W., Tomlinson, S.M., McCubbin, F.M., Greenwood, J.P., and Treiman, A.H. (2014)
572 The lunar apatite paradox. Science, 344, 400-402.
573 Burnham, C.W. (1994) Development of the Burnham model for prediction of H_2O solubility in
574 magmas. . In M. R. Carroll and J. R. Holloway, Eds., Volatiles in Magmas, 30, 123-129.
575 Reviews in Mineral¬ogy and Geochemistry, Mineralogical Society of America,
576 Chantilly, Virginia.
577 Carroll, M.R., and Webster, J.D. (1994) Solubilities of sulfur, noble gases, nitrogen, chlorine,
578 and fluorine in magmas. In M. R. Carroll and J. R. Holloway, Eds., Volatiles in Magmas,
579 231-279. Reviews in Mineralogy and Geochemistry, Mineralogical Society of America,
580 Chantilly, Virginia.
581 Colson, R.O. (1992) Mineralization on the Moon? Theoretical consideration of Apollo 16 "rusty
582 rocks", sulfide replacement in 67016 and surface-correlated volatiles on lunar volcanic
583 glasses. Proceedings of 22th Lunar and Planetary Science Conference, p. 427-436.
584 Dingwell, D.B., and Scarfe, C.M. (1985) Chemical diffusion of fluorine in melts in the system
585 Na_2O–Al_2O_3–SiO_2. Earth and Planetary Science Letters, 73, 377-384.
586 Dixon, J.E., Stolper, E.M., and Holloway, J.R. (1995) An experimental study of water and
587 carbon dioxide solubilities in mid-ocean ridge basaltic liquids. Journal of Petrology, 36,
588 1607-1631.
589 Elardo, S.M., McCubbin, F.M., and Shearer, C.K. (2012) Chromite symplectites in Mg-suite
590 troctolite 76535 as evidence for infiltration metasomatism of a lunar layered intrusion.
591 Geochimica et Cosmochimica Acta, 87, 154-177.
592 Elkins-Tanton, L.T., Chatterjee, N., and Grove, T.L. (2003) Magmatic processes that produced
593 lunar fire fountains. Geophysical Research Letters, 30, 1-4. doi:10.1029/2003GL017082.

Elkins-Tanton, L.T., and Grove, T. L. (2011) Water (hydrogen) in the lunar mantle: Results from petrology and magma ocean modeling. Earth and Planetary Science Letters, 307, 173-179.

Fegley, B.J. Jr. (1991) Thermodynamic models of the chemistry of lunar volcanic gases. Geophysical Research Letters, 18, 2073.

Fegley, B.J. Jr., and Swindle, T. D. (1993) In M. S. M. Lewis and M. L. Guerrieri, Eds., Resource of Near-Earth Space, 367-426. University of Arizona Press, Tucson Arizona.

Greenwood, J.P., Shoichi, I., Sakamato, N., Warren, P., Lawrence, T., and Hisayoshi, Y. (2011) Hydrogen isotope ratios in lunar rocks indicate delivery of cometary water to the Moon. Nature Geosciences, 4, 79-82.

Hauri, E.H., Weinreich, T., Saal, A.E., Rutherford, M.C., and Van Orman, J.A. (2011) High Pre-eruptive water contents preserved in lunar melt inclusions. Science, 333, 213-215.

Herd, C. D. K. (2008) Basalts as probes of planetary interior redox state. In G. J. MacPherson, D. W. Mittlefehldt, J. H. Jones, and S. B. Simon, Eds., Oxygen in the Solar System, 527-553. Reviews in Mineralogy and Geochemistry, Mineralogical Society of America, Chantilly, Virginia.

Hirschmann, M. M., Withers, A. C., Ardia, P., and Foley, N. T. (2012) Solubility of molecular hydrogen in silicate melts and consequences for volatile evolution of terrestrial planets. Earth and Planetary Science Letters, 345, 38-48.

Hui, H., Peslier, A., Zhang, Y., and Neal, C. R. (2013) Water in lunar anorthosites and evidence for a wet early Moon. Nature Geosciences, 6, 177-180.

615 Kiczenski, T.J., and Stebbins, J.F. (2006) The effect of fictive temperature on the structural
616 environment of fluorine in silicate and aluminosilicate glasses. Journal of American
617 Ceramic Society 89, 57-64.
618 Liu, Y., and Nekvasil, H. (2002) Si–F bonding in aluminosilicate glasses: Inferences from ab
619 initio NMR calculations. American Mineralogist, 87, 339–346.Mandeville, C.W.,
620 Webster, J.D., Rutherford, M.J., Taylor, B.E., Timbal, A., and Faure, K. (2002)
621 Determination of molar absorptivities for infrared absorption bands of H_2O in andesitic
622 glass. American Mineralogist, 87, 813-821.
623 Mathez, E.A., and Webster, J.D. (2005) Partitioning behavior of chlorine and fluorine in the
624 system apatite-silicate melt-fluid. Geochimica Cosmochimica Acta, 69, 1275-1286.
625 McCubbin, F.M., Steele, A., Hauri, E.H., Nekvasil, H., Yamashita, S., and Hemley, R.J. (2010a)
626 Nominally hydrous magmatism on the Moon. Proceedings of the National Academy of
627 Sciences, 107, 11223-11228.
628 McCubbin, F.M., Steele, A., Nekvasil, H., Schnieders, A., Rose, T., Fries, M., Carpenter, P. K.,
629 and Jolliff, B. L. (2010b) Detection of structurally bound hydroxyl in fluorapatite from
630 Apollo Mare basalt 15058,128 using TOF-SIMS. American Mineralogist, 95, 1141-1150.
631 McCubbin, F.M., Jolliff, B. L., Nekvasil, H., Carpenter, P. K., Zeigler, R. S., Steele, A., Elardo,
632 S. M., and Lindsley D.H. (2011) Fluorine and chlorine abundances in lunar apatite:
633 Implications for heterogeneous distributions of magmatic volatiles in the lunar interior.
634 Geochimica Cosmochimica Acta, 75, 5073-5093.
635 McCubbin, F.M., Hauri, E.H., Elardo, S.M., Vander Kaaden, K.E., Wang, J.H., and Shearer,
636 C.K. (2012) Hydrous melting of the martian mantle produced both depleted and enriched
637 shergottites. Geology, 40, 8, 683-686.

McCubbin, F.M., Elardo, S.M., Shearer Jr, C.K., Smirnov, A., Hauri, E.H., and Draper, D.S. (2013) A petrogenetic model for the co-magmatic origin of chassignites and nakhlites: Inferences from chlorine-rich minerals, petrology, and geochemistry. Meteoritics and Planetary Science, 48, 819-853.

McCubbin, F.M., Vander Kaaden, K.E., Tartèse, R., Klima, R.L., Liu, Y., Mortimer, J., Barnes, J.J., Shearer, C.K., Treiman, A.H., Lawrence, D.J., Elardo, S.M., Hurley, D.M., Boyce, J.W., and Anand, M. (2015a) Magmatic volatiles (H, C, N, F, S, Cl) in the lunar mantle, crust, and regolith: Abundances, distributions, processes, and reservoirs. American Mineralogist, 100, In Press.

McCubbin, F.M., Vander Kaaden, K.E., Tartèse, Boyce, J.W., Mikhail, S., Whitson, E.S., Bell, A.S., Anand, M., Franchi, I.A., Wang, J., and Hauri, E.H. (2015b) Experimental investigation of F, Cl, and OH partitioning between apatite and Fe-rich basaltic melt at 1.0-1.2 GPa and 950-1000 °C. American Mineralogist, 100, In Revision.

McKay, D.S., and Wentworth, S.J. (1992) Morphology and Composition of Condensates on Apollo 17 Orange and Black Glasses. Lunar and Planetary Institute Technical Report Part I. 92-09.

Mysen, B.O., Cody, G.D., and Smith, A. (2004) Solubility mechanisms of fluorine in peralkaline and meta-aluminous silicate glasses and in melts to magmatic temperatures Geochimica Cosmochimica Acta 68, 2745–2769.

Meyer C., McKay D.S., Anderson D.H., and Butler P. (1975) The source of sublimates on the Apollo 15 green and Apollo 17 orange glass samples. Proceedings of 6th Lunar and Planetary Science Conference, 1673-1699.

660 Neal C.R., and Kramer G.Y. (2006) The petrogenesis of the Apollo 14 high-Al mare basalts.
661 American Mineralogist, 91, 1521-1535.
662 Neal, C.R., Taylor, L.A., and Patchen, A.D. (1989) High alumina (HA) and very high potassium
663 (VHK) basalt clasts from Apollo 14 breccias. Proceedings of 19th Lunar and Planetary
664 Science Conference, 23.
665 Nekvasil, H., McCubbin, F.M., and Ustunisik G. (2011) Magmatic degassing in planetary
666 bodies: What apatite can tell us. Proceedings of 42nd Lunar and Planetary Science
667 Conference, 2240.
668 Robinson, K.L. and Taylor, G.J. (2014) Heterogeneous distribution of water in the Moon. Nature
669 Geoscience, 7, 401-408. doi:10.1038/ngeo2173.
670 Saal, A. E., Hauri, E.H., Lo Cascio, M., Van Orman, J. A., Rutherford, M. C., and Cooper, R. F.
671 (2008) Volatile content of lunar volcanic glasses and the presence of water in the Moon's
672 interior. Nature, 454, 192-195.
673 Saal, A. E., Hauri, E.H., Van Orman, J. A., and Rutherford M. C. (2013) Hydrogen isotopes in
674 lunar volcanic glasses and melt inclusions reveal a carbonaceous chondrite heritage.
675 Science, 340, 1317-1320.
676 Sandland, T.O., D.L., Stebbins, J.F., and Webster, J.D. (2004) Structure of Cl-containing silicate
677 and aluminosilicate glasses: A 35Cl MAS-NMR study. Geochimica Cosmochimica Acta
678 68, 5059-5069.
679 Schaller, T., D.D.B., Keppler, H., Knöller, W., Merwin, L., and Sebald, A. (1992) Fluorine
680 insilicate glasses: A multinuclear nuclear magnetic resonance study. Geochimica
681 Cosmochimica Acta 56, 701-707.Sharp, Z.D., Barnes, J.D., Brearley, A.J., Chaussidon,

682 M., Fischer, T.P., and Kamenetsky, V.S. (2007) Chlorine isotope homogeneity of the
683 mantle, crust and carbonaceous chondrites. Nature, 446, 7139, 1062-1065.
684 Sharp, Z.D., Shearer C.K., McKeegan K.D. Barnes, J.D., and Wang Y.Q. (2010) The chlorine
685 isotope composition of the Moon and implications for an anhydrous Mantle. Science,
686 329, 1050-1053.
687 Sharp, Z.D., McCubbin, F.M., and Shearer, C.K. (2013a) A hydrogen-based oxidation
688 mechanism relevant to planetary formation. Earth and Planetary Science Letters, 380, 88-
689 97.
690 Sharp, Z.D., Mercer, J.A., Jones, R.H., Brearley, A.J., Selverstone, J., Bekker, A., and Stachel, T.
691 (2013b) The chlorine isotope composition of chondrites and Earth. Geochimica et
692 Cosmochimica Acta, 107, 189-204.
693 Shearer, C.K., Burger, P.V., Guan, Y., Papike, J.J., Sutton, S.R., and Atudorei, N.V. (2012)
694 Origin of sulfide replacement textures in lunar breccias. Implications for vapor element
695 transport in the lunar crust. Geochimica et Cosmochimica Acta, 83, 138-158.
696 Shearer, C.K., Sharp, Z.D., Burger, P.V., McCubbin, F.M., Provencio, P.P., Brearley, A.J., and
697 Steele, A. (2014) Chlorine distribution and its isotopic composition in “rusty rock”
698 66095. Implications for volatile element enrichments of “Rusty Rock” and lunar soils,
699 origin of “rusty” alteration, and volatile element behavior on the Moon. Geochimica et
700 Cosmochimica Acta, 139, 411-433.
701 Shearer, C.K., Elardo, S.M., Petro, N.E., Borg, L.E., and McCubbin, F.M. (2015) Origin of the
702 lunar highlands Mg-suite plutonic rocks. An integrated petrology, geochemistry,
703 chronology, and remote sensing perspective. American Mineralogist, 100, 294-325.

Signorelli S., and Carroll M. R. (2000) Solubility and fluid-melt partitioning of Cl in hydrous phonolitic melts. Geochimica Cosmochimica Acta 64, 2851-2862.

Signorelli S. and Carroll M. R. (2002) Experimental study of Cl solubility in hydrous alkaline melts: Constraints on the theoretical maximum amount of Cl in trachytic and phonolitic melts. Contributions to Mineralogy and Petrology 143, 209-218.

Tartèse, R., and Anand, M. (2013) Late delivery of chondritic hydrogen into the lunar mantle: Insights from mare basalts. Earth and Planetary Science Letters, 361, 480-486.

Tartèse, R., Anand, M., Barnes, J.J., Starkey, N.A., Franchi, I.A., and Sano, Y. (2013) The abundance, distribution, and isotopic composition of Hydrogen in the Moon as revealed by basaltic lunar samples: Implications for the volatile inventory of the Moon. Geochimica et Cosmochimica Acta, 122, 58-74.

Tartèse, R., Anand, M., McCubbin, F.M., Elardo, S.M., Shearer Jr, C.K., and Franchi, I.A. (2014) Apatites in lunar KREEP basalts: The missing link to understanding the H isotope systematics of the Moon. Geology, 42, 363-366.

Taylor, L.A., Patchen, A., Mayne, R.G., and Taylor, D.H. (2004) The most reduced rock from the moon, Apollo 14 basalt 14053: Its unique features and their origin. American Mineralogist, 89, 1617-1624.

Treiman, A.H., Boyce, J.W., Gross, J., Guan, Y., Eiler, J., and Stolper, E.M. (2014) Phosphate-halogen metasomatism of granulite 79215: Impact-induced fractionation of lunar volatiles and incompatible elements. American Mineralogist, 99, 1860-1870.

Ustunisik G., Nekvasil H., and Lindsley D.H. (2011a) Differential degassing of H_2O, Cl, F, and S: Potential effects on lunar apatite. American Mineralogist, 96, 1650-1653.

726 Ustunisik G., Nekvasil H., and Lindsley D.H. (2011b) Experimental determination of degassing
727 pathways from lunar magmas: New Insights from time studies. Proceedings of a Wet
728 versus Dry Moon Meeting, 6018.
729 Wang, Y., Guan, Y., Hsu, W., and Eiler, J.M. (2012) Water content, chlorine and hydrogen
730 isotope compositions of lunar apatite. Proceedings of the 75th Annual Meteoritical
731 Society Meeting, 5170.
732 Watson, E.B. (1994) Diffusion in volatile-bearing magmas. In M. R. Carroll and J. R. Holloway,
733 Eds., Volatiles in Magmas, 371-411. Reviews in Mineralogy and Geochemistry,
734 Mineralogical Society of America, Chantilly, Virginia.
735 Webster J. D., Kinzler R. J., and Mathez A. (1999) Chloride and water solubility in basalt and
736 andesite melts and implications for magmatic degassing. Geochimica Cosmochimica
737 Acta 63, 729-738.
738 Webster J. D., and De Vivo B. (2002) Experimental and modeled solubilities of chlorine in
739 aluminosilicate melts, consequences of magma evolution and implications for exsolution
740 of hydrous chloride melt at Mt. Somma-Vesuvius. American Mineralogist 87, 1046-1061.
741 Wetzel, D.T., Rutherford, M.J., Jacobsen, S.D., Hauri, E.H., and Saal, A.E. (2013) Degassing of
742 reduced carbon from planetary basalts. Proceedings of the National Academy of
743 Science, 110, 8010-8013.
744 Willis, J.P., Erlank, A.J., Gurney, J.J., Theil, R.H., and Ahrens, L.H. (1972) Major, minor, and
745 trace element data for some Apollo 11, 12, 14 and 15 samples. Proceedings of 3rd Lunar
746 and Planetary Science Conference.

Witter, J. B., and Kuhner, S. M. (2004) A simple empirical method for high-quality electron microprobe analysis of fluorine at trace levels in Fe-bearing minerals and glasses. American Mineralogist, 89, 57-63.

Zeng, Q., and Stebbins, J.F. (2000) Fluoride sites in aluminosilicate glasses: High-resolution ^{19}F NMR results. American Mineralogist, 85, 863-867.

Zhang, Y., and Ni, H. (2010) Diffusion of H, C, and O components in silicate melts. In Y. Zhang and D. J. Cherniak, Eds., Diffusion in Minerals and Melts, 171-225. Reviews in Mineralogy and Geochemistry, Mineralogical Society of America, Chantilly, Virginia.

Zhang, Y., Ni, H., and Chen, Y. (2010) Diffusion data in silicate melts. In Y. Zhang and D. J. Cherniak, Eds., Diffusion in Minerals and Melts, 311-408. Reviews in Mineralogy and Geochemistry, Mineralogical Society of America, Chantilly, Virginia.

Figure Captions

Figure 1. Back-scattered electron (BSE) images of initial (M_I) and final degassed glasses after 10 minutes (M_{F10min}), 1 hour (M_{F1h}), 4 hours (M_{F4h}), 6 hours (M_{F6h}) of single-step and 1+3 hour (M_{F1+3h}) and 4+2 hour (M_{F4+2h}) of two-step degassing. Numbers shows the location of point analysis from each run product at single-step degassing experiments. Both initial and final degassed glasses are completely crystal-free. Irregular white blobs around the edges of the experimental glasses in 1, 4 and 6 hours single-step and 1+3h and 4+2h two-step degassing

767 experiments indicate the metallic Fe (FeO^r) droplets due to the shift in oxygen fugacity between
768 high-P synthesis and low-P degassing experiments.

769 **Figure 2.** Percentage of volatiles lost from the initial melt as a function of degassing time for
770 bulk degassing, PATHs A-D (arrows to solid symbols shown for fluorine). Similar arrows could
771 be drawn for each volatile component. PATH E is the incremental path from 1 to 4 hours. PATH
772 F is the incremental path from 4 to 6 hours. Dashed lines show variation in percentage loss as a
773 function of time along the time segment 10 minutes to 6 hours for bulk degassing. The effective
774 degassing time for Path F is based on consistency with loss of Cl and S in the bulk degassing
775 steps at 4 and 6 hours (symbols with gray outlines).

776 **Figure 3.** Schematic indicating changes in the system through the formation of volatile phases
777 (and metallic Fe) during bulk (single-step) degassing (Paths A-D) and sequential (two-step)
778 degassing (Path E and F). Measured volatile contents of melt (M) are given in the gray boxes.
779 Computed sequential contributions to the volatile phase (s) (V), based on the differences in bulk
780 V between sequential time steps from bulk degassing experiments are indicated above each box.
781 The volatile phase V produced along path E reflects that exsolved when the melt from path B is
782 allowed to degas nominally for an additional three hours The volatile phase V produced along
783 path F reflects that exsolved when the melt from path C is allowed to degas nominally for an
784 additional two hours. All compositions are in ppm. The number of numerical digits shown goes
785 beyond those that are significant for comparative purposes

786 **Figure 4.** Changes in computed incremental volatile phase composition after loss of water (at 10
787 minutes). Compositions plotted reflect integrated changes in composition over entire time
788 interval between successive bulk degassing times (e.g., the point plotted at 1 hour shows the net

addition of vapor phase exsolved between 10 minutes and 1 hour to the vapor exsolved at 10 minutes). The net time for the two-step process (symbols with gray outline) is that from Figure 2.

Figure 5a. Relative volatile abundances of OH, Cl, and F in initial melt (M_I) and final degassed melt after bulk degassing at 10 minutes (M_{F10min}), 1 hour (M_{F1h}), 4 hours (M_{F4h}), and 6 hours (M_{F6h}) for the paths of Figure 3 (black arrows). Note that M_{F1h} is the initial melt (M_{I1+3h}) for two-step degassing of 1+3h and M_{F4h} is the initial melt (M_{I4+2h}) for two-step degassing of 4+2h. The co-existing melt (M_{F1+3h}) from degassing of M_{I1h} is indicated by pattern-filled triangles. The co-existing melt (M_{F4+2h}) from degassing of M_{I4h} is indicated by solid-filled triangles.

Figure 5b. Computed relative volatile content of the co-existing bulk volatile phase after 10 minutes (V_{10min}), 1 hour (V_{1h}), 4 hours (V_{4h}), and 6 hours (V_{6h}) degassing. The computed incremental volatile phase added to the bulk volatile phase during a specific time interval is indicated by light gray symbols and labeled as ΔV_{com} with the time interval indicated (e.g., $\Delta V_{com10min-1h}$). Note that V_{10min} can also be considered as $\Delta V_{com0-10min}$. Dashed tie-lines show geometrically the relative proportions of the incremental volatile phase ($\Delta V_{com\ time\ a\ -\ time\ b}$) added to the bulk volatile phase of the previous time step ($V_{time\ a}$). The computed volatile phase ($V_{exp1+3h}$) from degassing of M_{I1h} is indicated by pattern-filled triangles. The computed volatile phase ($V_{exp4+2h}$) from degassing of M_{I4h} is indicated by solid-filled triangles.

Figure 5c. Relative volatile abundances of OH, Cl, and F in hypothetical apatites in equilibrium with the initial melt (Ap_I) and final degassed melts (Ap_t) for t=10 minutes, 1 hour, 4 hours, and 6 hours of bulk degassing. The black arrows show the direction of hypothetical apatite evolution from initial to degassed compositions for the bulk degassing paths. The dashed arrow shows the F:Cl ratio of the hypothetical apatite in the undegassed melt.

811 **Figure 6.** Estimated $\delta^{37}Cl$ (open symbols) of melt after 10 minutes, 1 hour, 4 hours, and 6 hours
812 degassing of $FeCl_2$, assuming that within the first 10 minutes Cl was lost as HCl and resulted in
813 no isotopic effect (and hence, retention of the value the bulk rock value of 0‰). The computed
814 fraction of Cl remaining (F), after each degassing experiment is relative to the Cl content of the
815 melt after 10 minutes degassing, and is plotted on the calculated trajectory of $\delta^{37}Cl$ values during
816 degassing of $FeCl_2$ vapor species from Sharp et al. (2010).

FIGURE 1.

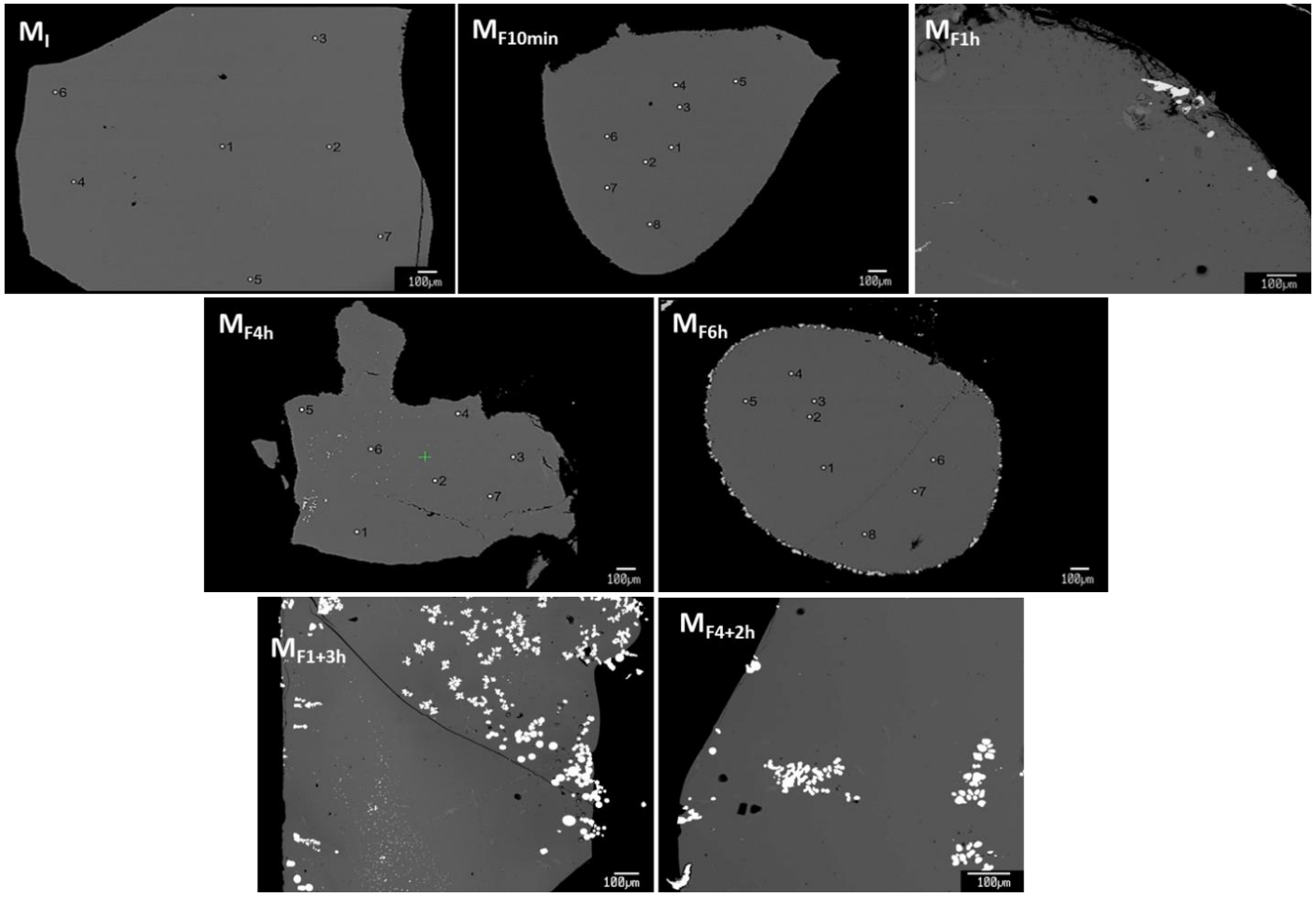

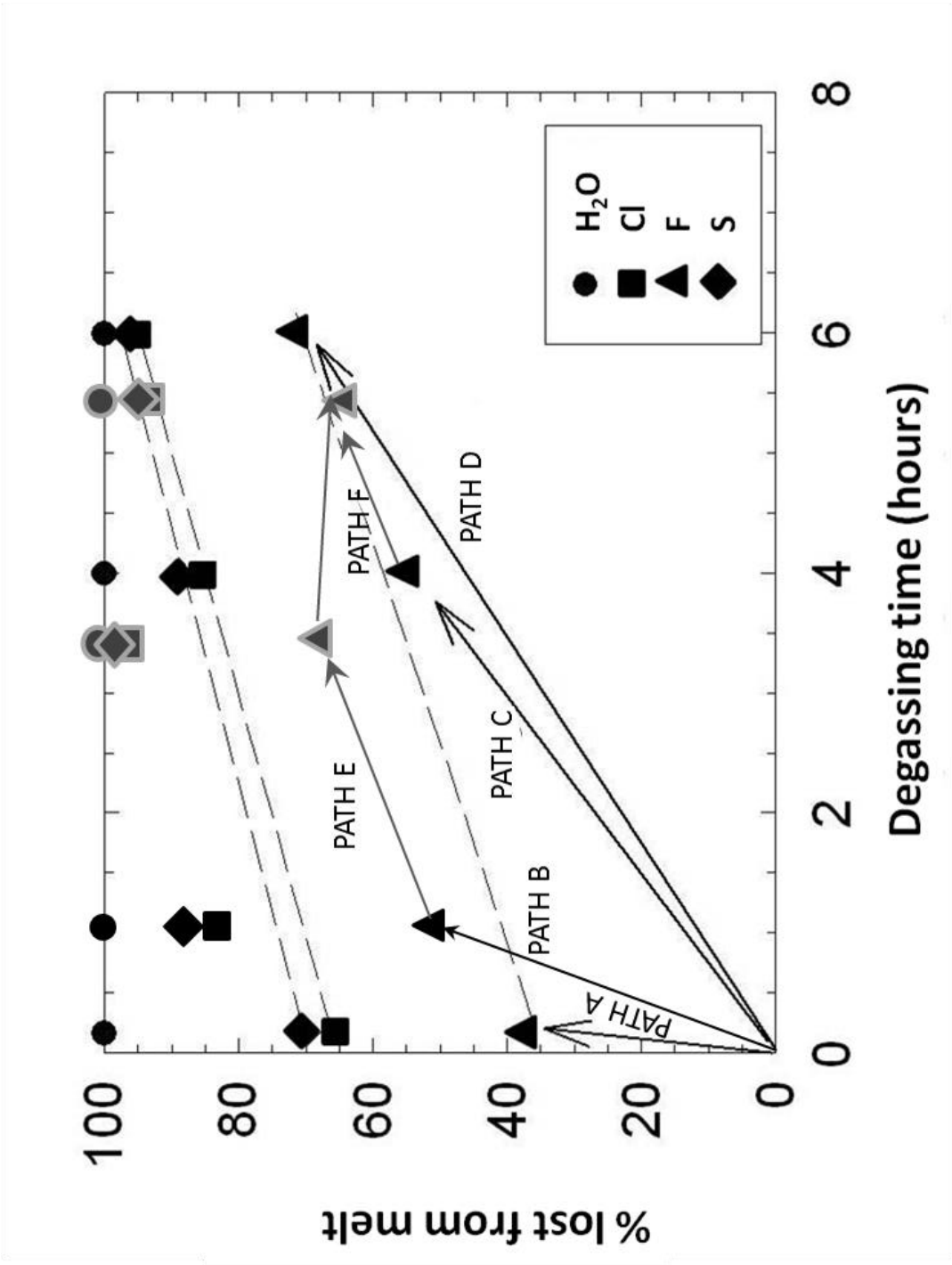
% lost from melt
100
80
60
40
20
0
0
2
4
6
8
Degassing time (hours)
H2O
Cl
F
S
PATH A
PATH B
PATH C
PATH D
PATH E
PATH F

FIGURE 2.

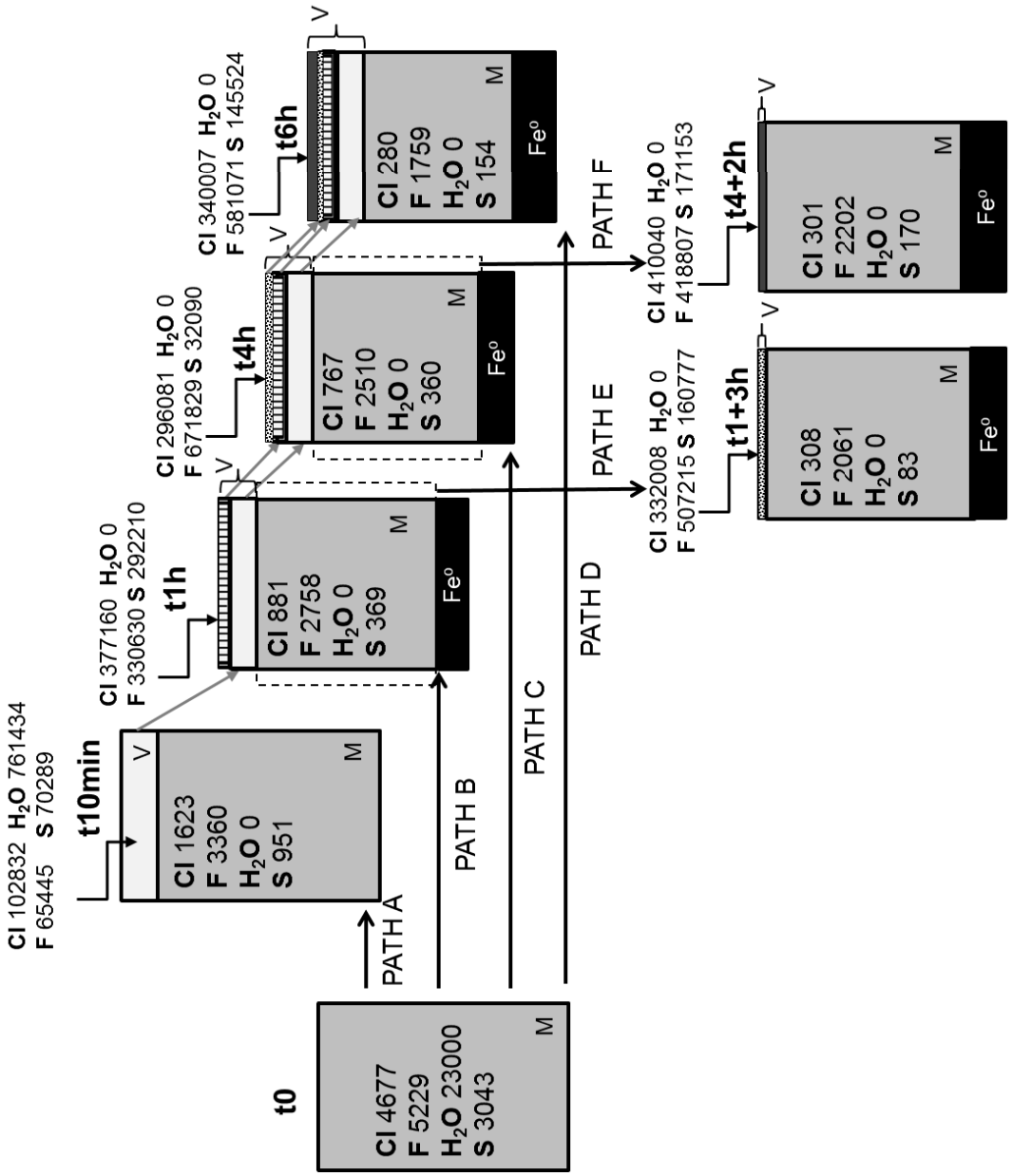
t0
Cl 4677
F 5229
H2O 23000
S 3043
M
PATH A
PATH B
PATH C
PATH D
PATH E
PATH F
t10min
Cl 102832 H2O 761434
F 65445 S 70289
V
Cl 1623
F 3360
H2O 0
S 951
M
t1h
Cl 377160 H2O 0
F 330630 S 292210
Cl 881
F 2758
H2O 0
S 369
Fe°
t4h
Cl 296081 H2O 0
F 671829 S 32090
Cl 767
F 2510
H2O 0
S 360
t6h
Cl 340007 H2O 0
F 581071 S 145524
Cl 280
F 1759
H2O 0
S 154
t1+3h
Cl 332008 H2O 0
F 507215 S 160777
Cl 308
F 2061
H2O 0
S 83
t4+2h
Cl 410040 H2O 0
F 418807 S 171153
Cl 301
F 2202
H2O 0
S 170

FIGURE 3.

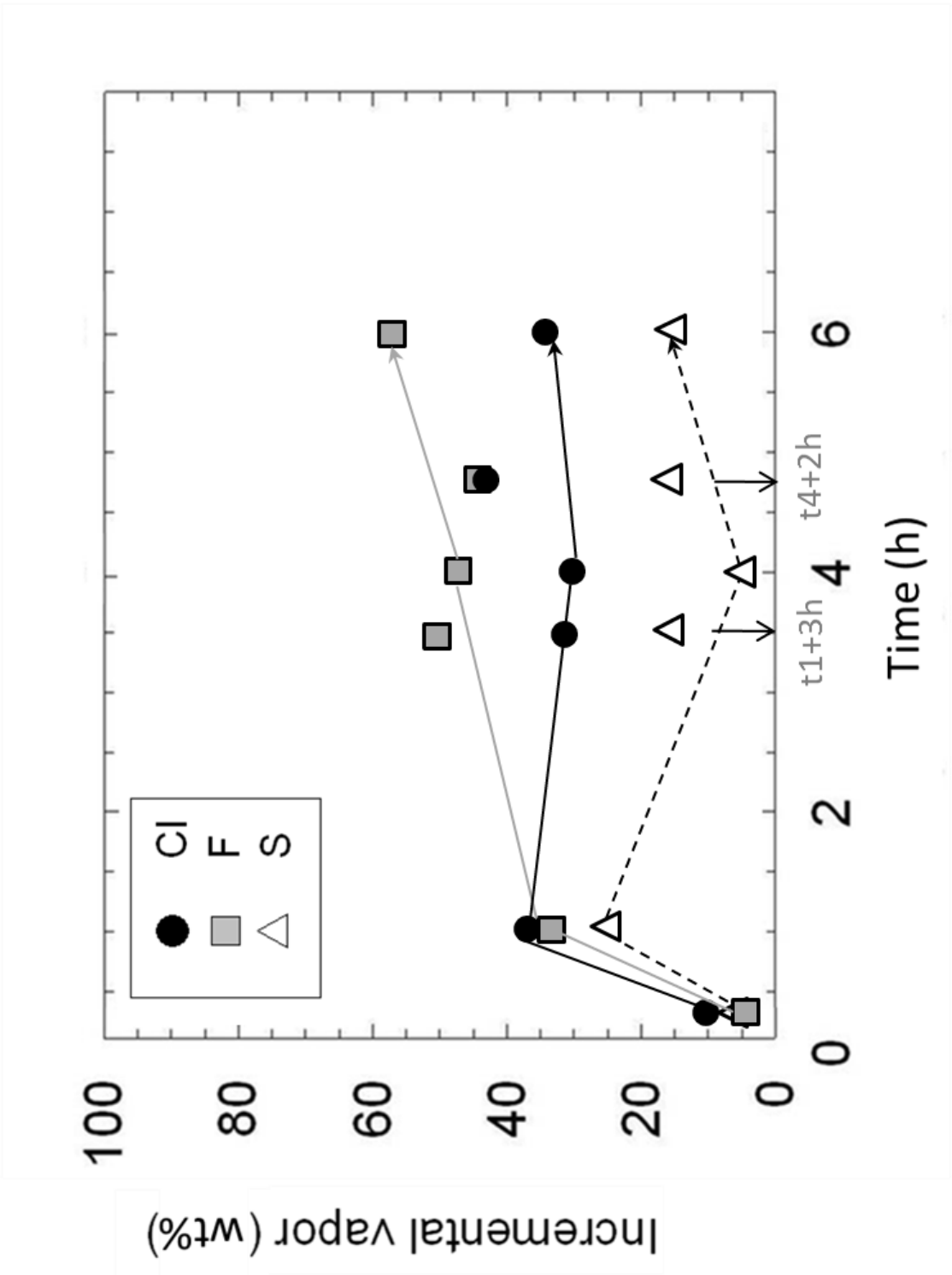
Incremental vapor (wt%)
100
80
60
40
20
0
0
2
4
6
Time (h)
t1+3h
t4+2h
Cl
F
S

FIGURE 4.

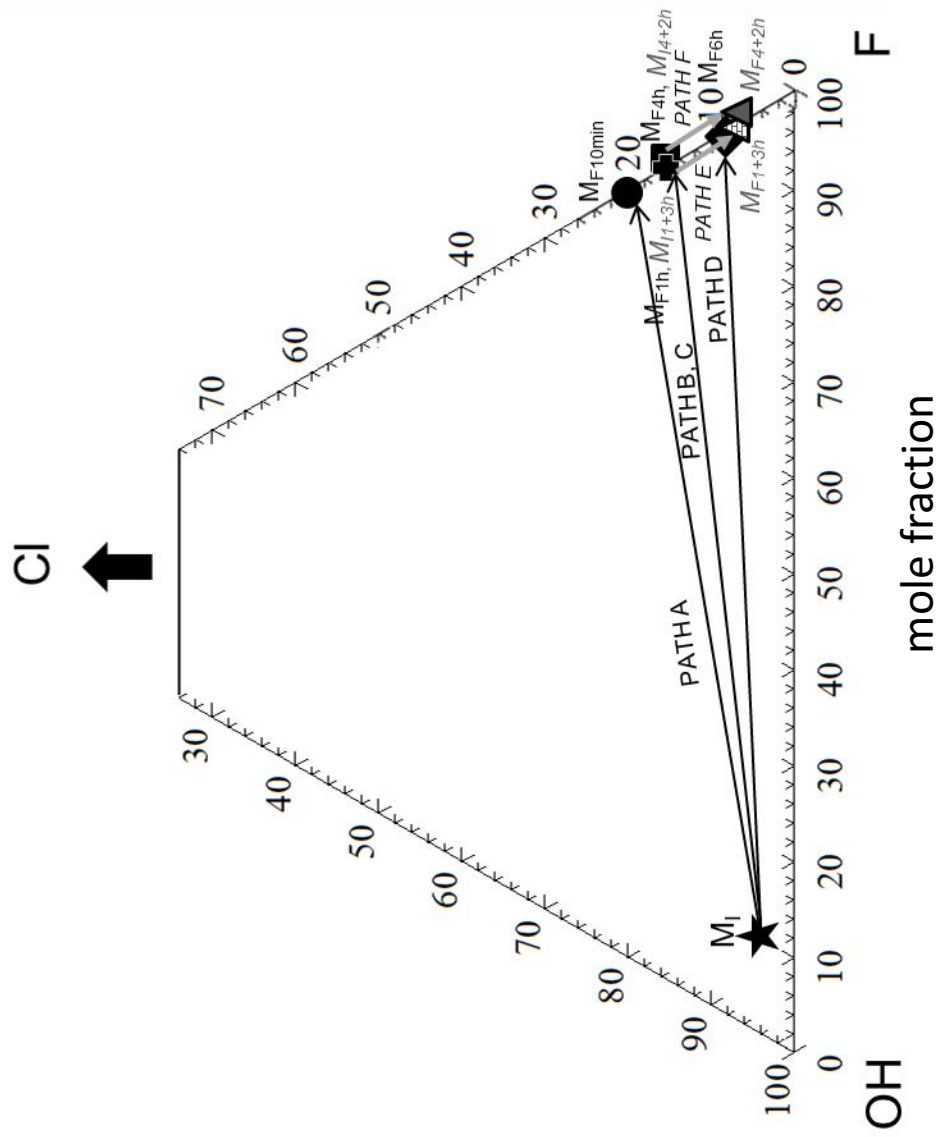
Cl
F
OH
mole fraction
PATH A
PATH B, C
PATH D
PATH E
PATH F
M_{F10min}
M_{F4h}, M_{I4+2n}
M_{F1h}, M_{I1+3n}
M_{F6h}
M_{F4+2n}
M_{F1+3n}
M_I

FIGURE 5a.

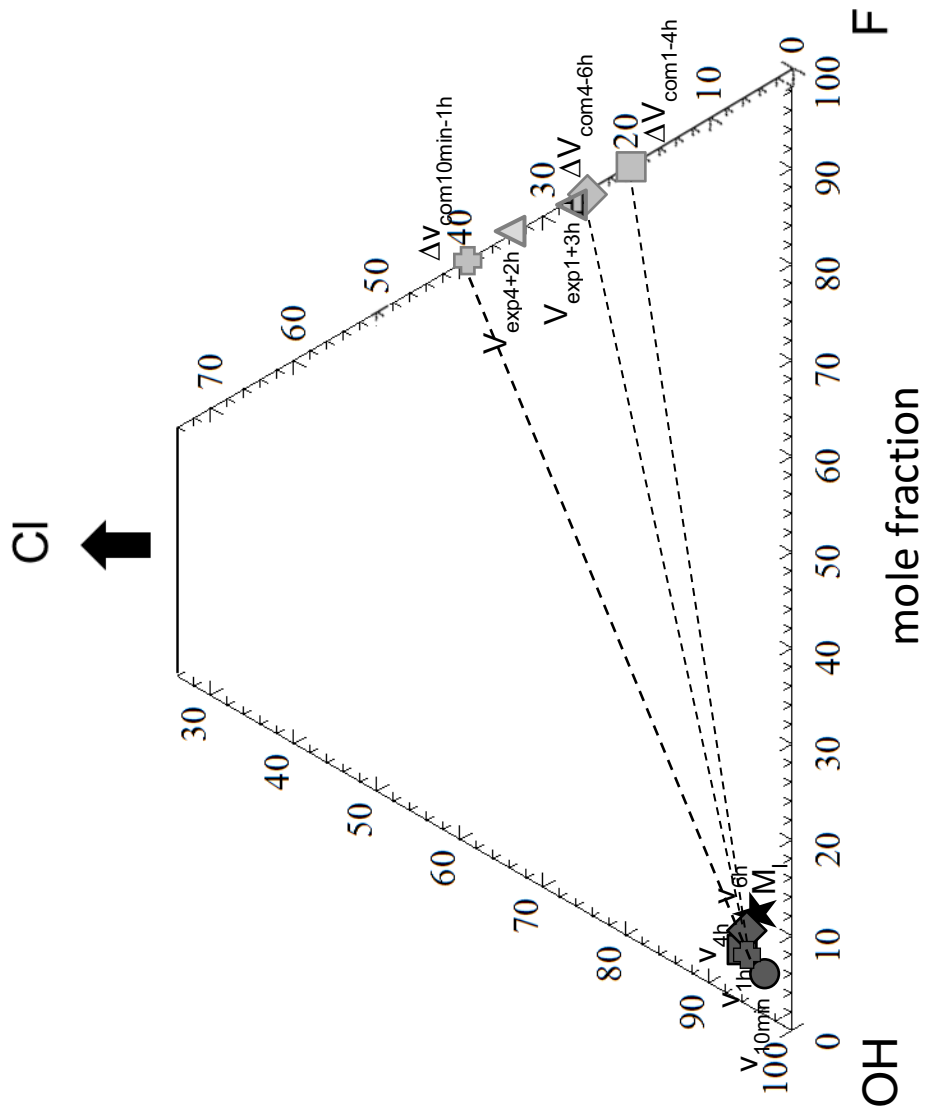
Cl
OH
F
mole fraction
0
10
20
30
40
50
60
70
80
90
100
$\Delta V_{com10min-1h}$
$\Delta V_{exp4+2h}$
$\Delta V_{exp1+3h}$
$\Delta V_{com4-6h}$
$\Delta V_{com1-4h}$
V_{10min}
V_{1h}
V_{4h}
V_{6h}
M_I

FIGURE 5b.

FIGURE 5c.

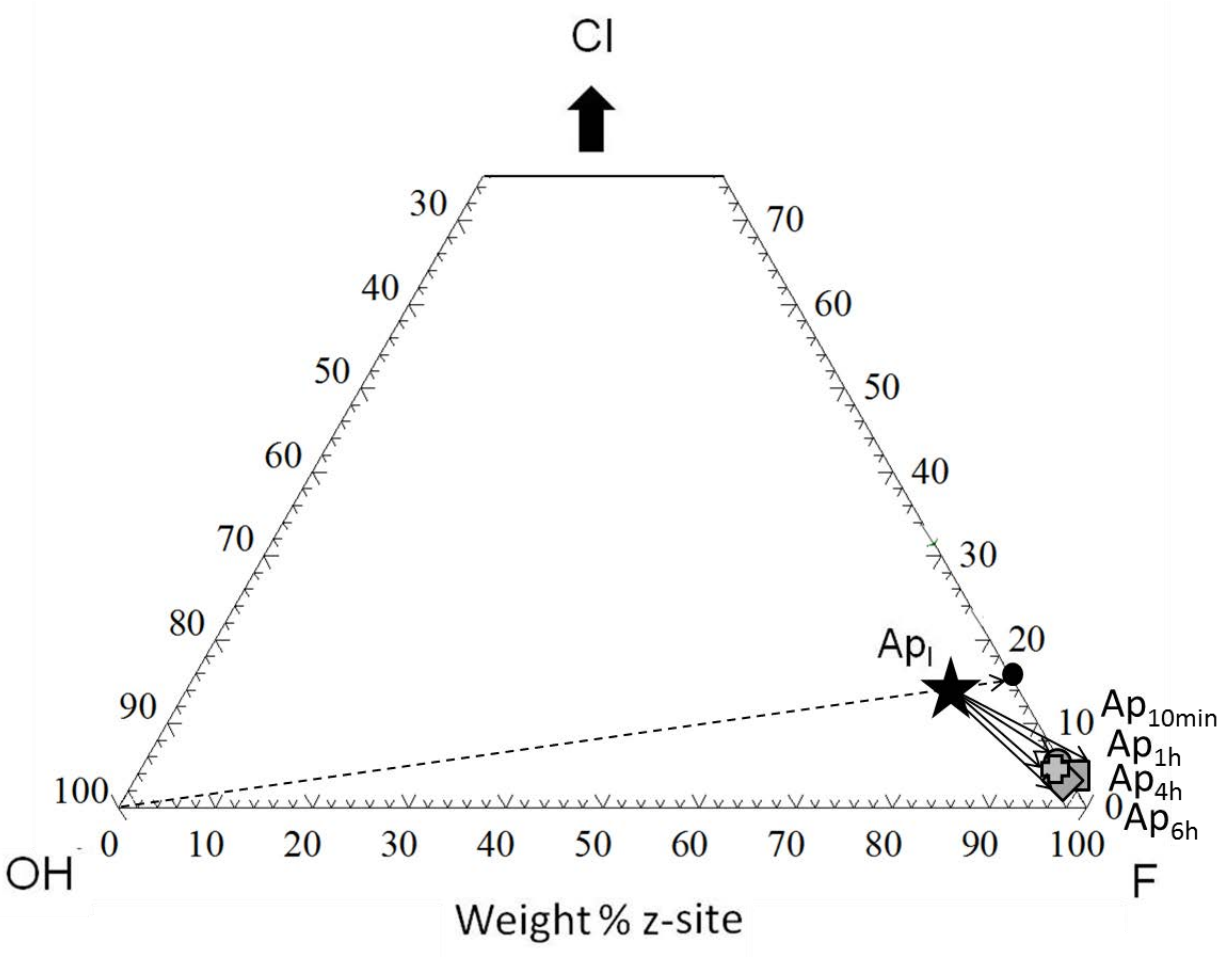
Cl
30
40
50
60
70
80
90
100
70
60
50
40
30
20
10
0
Ap$_I$
Ap$_{10min}$
Ap$_{1h}$
Ap$_{4h}$
Ap$_{6h}$
0
10
20
30
40
50
60
70
80
90
100
OH
F
Weight % z-site

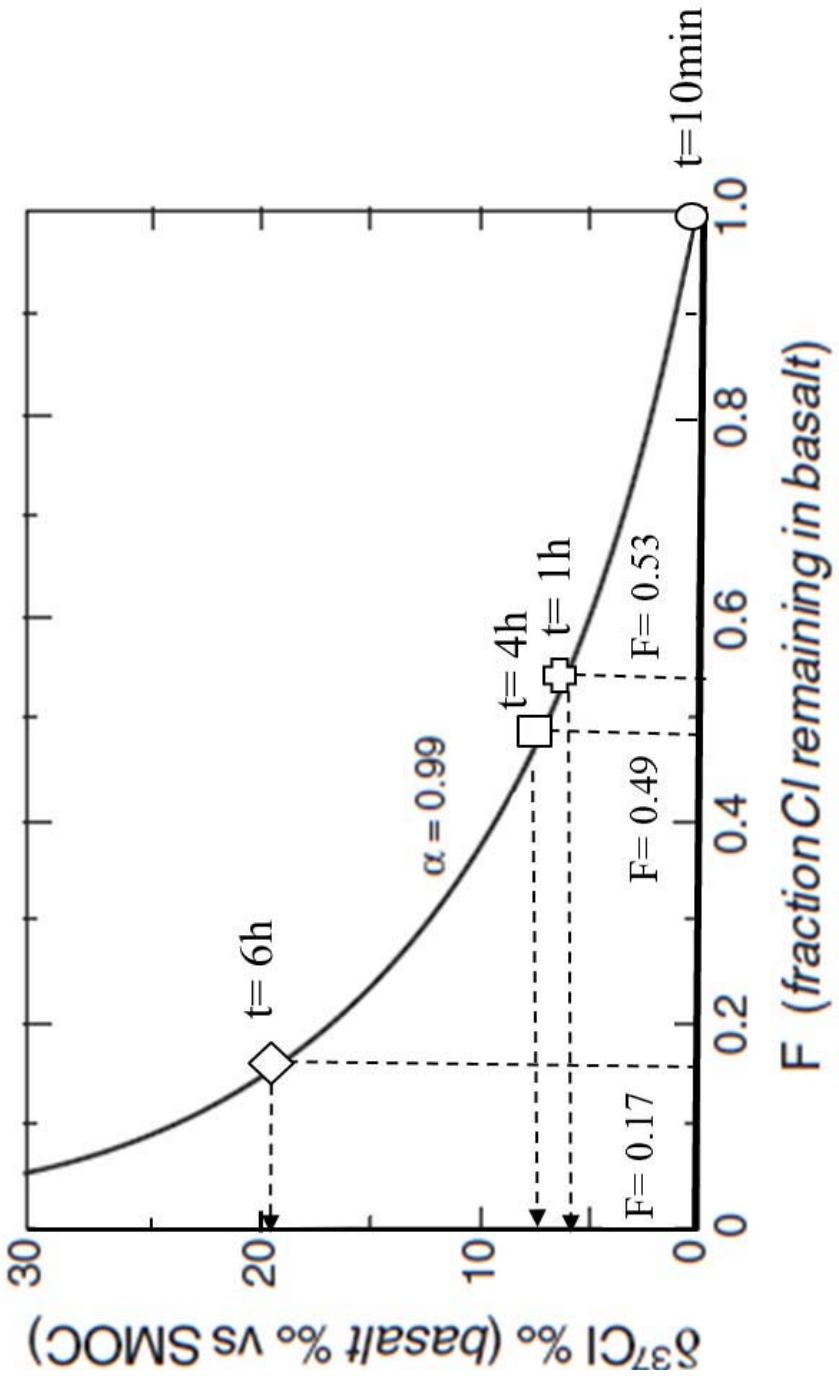
t=10min
t= 1h
t= 4h
t= 6h
α = 0.99
F= 0.53
F= 0.49
F= 0.17
F (fraction Cl remaining in basalt)
δ37Cl ‰ (basalt ‰ vs SMOC)
0
0.2
0.4
0.6
0.8
1.0
30
20
10
0

FIGURE 6.

TABLE 1. Target composition (14053) and mean compositions of initial, final, and Fe^0 corrected (Fe^0 corr.) degassed melts.

	Target[a]	Initial (t0)	Final (t10min)[d]	Final (t1h)	Fe^0 corr. Final (t1h)[e]	Final (t4h)	Fe^0 corr. Final (t4h)[f]	Final (t6h)	Fe^0 corr. Final (t6h)	Final (t1+3h)	Fe^0 corr. Final (t1+3h)	Final (t4+2h)	Fe^0 corr. Final (t4+2h)
SiO_2[b]	45.86	46.04 (*0.29*)[c]	46.73 *(0.21)*	48.16 *(0.32)*	46.90	48.98 *(0.41)*	46.83	52.5 *(0.18)*	47.08	53.87 *(0.60)*	45.98	54.1 *(0.48)*	46.84
TiO_2	2.9	2.77 (*0.02*)	2.49 *(0.12)*	2.55 *(0.11)*	2.48	2.8 *(0.11)*	2.68	3.08 *(0.03)*	2.76	3.38 *(0.22)*	2.89	3.18 *(0.15)*	2.75
Al_2O_3	12.48	12.74 (*0.07*)	12.83 *(0.06)*	13.34 *(0.05)*	13.01	13.59 *(0.14)*	12.99	14.41 *(0.06)*	12.92	14.99 *(0.11)*	12.81	14.76 *(0.12)*	12.78
FeO_T	16.89	16.83 (*0.17*)	16.86 *(0.15)*	14.97 *(0.26)*	17.21	13.53 *(0.86)*	17.31	7.8 *(0.06)*	17.33	3.50 *(0.20)*	17.62	5.12 *(0.38)*	17.86
MgO	8.93	9.23 (*0.08*)	9.69 *(0.07)*	9.68 *(0.14)*	9.42	9.45 *(0.19)*	9.03	10.45 *(0.09)*	9.37	11.57 *(0.26)*	9.88	10.64 *(0.10)*	9.21
CaO	11.02	10.39 (*0.06*)	10.23 *(0.08)*	10.43 *(0.06)*	10.16	10.88 *(0.10)*	10.40	11.34 *(0.04)*	10.17	12.15 *(0.19)*	10.37	11.69 *(0.06)*	10.12
Na_2O	0.44	0.43 (*0.01*)	0.39 *(0.01)*	0.34 *(0.01)*	0.33	0.31 *(0.01)*	0.30	0.17 *(0.01)*	0.15	0.23 *(0.02)*	0.20	0.19 *(0.02)*	0.16
K_2O	0.1	0.11 (*0.01*)	0.09 *(0.01)*	0.07 *(0.01)*	0.07	0.05 *(0.01)*	0.05	0.03 *(0.00)*	0.02	0.04 *(0.01)*	0.04	0.04 *(0.00)*	0.04
P_2O_5	0.11	0.13 (*0.01*)	0.09 *(0.01)*	0.04 *(0.02)*	0.04	0.04 *(0.01)*	0.04	0.01 *(0.00)*	0.01	0.01 *(0.01)*	0.01	0.01 *(0.01)*	0.01
Cl	5000	4787 (*49*)	1623 *(82)*	881 *(58)*	858	767 *(95)*	733	280 *(28)*	251	307 *(57)*	263	301 *(54)*	260
F	5000	5352 (193)	3360 *(106)*	2758 *(115)*	2686	2510 *(140)*	2399	1759 *(253)*	1577	2061 *(194)*	1760	2202 *(174)*	1907
S	3000	3115 (326)	951 *(820)*	369 *(73)*	359	360 *(50)*	344	154 *(37)*	138	83 *(44)*	71	170 *(43)*	147
Total	100	100	100	100	100	100	100	100	100	100	100	100	100
H_2O	-	2.3 (*0.1*)	0 *(0.01)*	0 *(0.01)*	0	0 *(0.01)*	0	0 *(0.01)*	0	0 *(0.01)*	0	0 *(0.01)*	0

Note: [a]Willis et al. 1972.
[b]Oxides and water in wt%; Cl, F, S in ppm.
[c](1σ).
[d]10 minutes bulk degassing experimental products do not contain metallic Fe (FeO^r).
[e]Fe^0 corrected Final (t1h) is the initial composition for t1+3h sequential degassing.
[f]Fe^0 corrected Final (t4h) is the initial composition for t4+2h sequential degassing.

TABLE 2. Mass balance results.

			WF[a]	Cl	F	S	H_2O
t10min	Vapor	Composition (ppm)		102832	65445	70289	761434
	Final Melt	Volatile abundance (ppm)		1623	3360	951	0
		Volatile loss (%)		66	38	70	100
	Contribution to the system (ppm)	Vapor	0.030200	3106	1976	2123	22995
		Melt	0.969800	1574	3259	922	0
t1h	Vapor	Composition (ppm)		119535	81592	83801	715072
	Final Melt	Volatile abundance (ppm)		881	2758	369	0
		Volatile loss (%)		82	50	89	100
	Contribution to the system (ppm)	Vapor	0.032249	3855	2631	2702	23060
		Melt	0.944800	833	2606	348	0
t4h	Vapor	Composition (ppm)		121703	88842	83166	706289
	Final Melt	Volatile abundance (ppm)		767	2510	360	0
		Volatile loss (%)		85	55	89	100
	Contribution to the system (ppm)	Vapor	0.032586	3966	2895	2710	23015
		Melt	0.928640	712	2331	334	0
t6h	Vapor	Composition (ppm)		130235	108582	85472	675711
	Final Melt	Volatile abundance (ppm)		280	1759	154	0
		Volatile loss (%)		95	71	96	100
	Contribution to the system (ppm)	Vapor	0.034108	4442	3704	2915	23047
		Melt	0.869290	243	1529	134	0
t1+3h	Vapor	Composition (ppm)		332008	507215	160777	0
	Final Melt	Volatile abundance (ppm)		308	2061	83	0
		Volatile loss (%)		69	34	80	
	Contribution to the system (ppm)	Vapor	0.001517	504	770	244	0
		Melt	0.856362	263	1765	71	0
t4+2h	Vapor	Composition (ppm)		410040	418807	171153	0
	Final Melt	Volatile abundance (ppm)		301	2202	170	0
		Volatile loss (%)		64	20	57	
	Contribution to the system (ppm)	Vapor	0.001230	504	515	211	0
		Melt	0.910100	274	2004	154	0

Note: [a]weight fraction of phase in system (only vapor and melt are given, not FeO^r); digits beyond two decimal places are given only for mass balance purposes.

TABLE 3. Compilation of diffusion coefficients (D) from the literature for each of the volatile components (H_2O, F, Cl, S) in our experiments.

	Melt Composition	H_2O_{melt} (wt.%)	T (K)	D (m^2/s)	Reference
H_2O^T	Basalt	2.3	1523	1.57×10^{-9}	Zhang and Ni,(2010)
F	Basalt	3.0	1523	3.67×10^{-11}	Alletti et al., (2007)
Cl	Basalt	3.0	1523	2.92×10^{-11}	Alletti et al., (2007)
S	Basalt	2.3	1523	9.23×10^{-12}	Zhang et al., (2010)
H_2O^T	Basalt	0.01	1523	6.81×10^{-12}	Zhang and Ni, (2010)
F	Basalt	0.00	1523	1.94×10^{-11}	Alletti et al., (2007)
Cl	Basalt	0.00	1523	1.03×10^{-11}	Alletti et al., (2007)
S	Basalt	0.01	1523	3.47×10^{-12}	Zhang et al., (2010)

Note: ^{T}Includes all molecular forms of H^+